Generalized Time Slot Index Modulation for Optical Wireless Communications

Generalized Time Slot Index Modulation for Optical Wireless Communications

Ardimas Andi Purwita, *Student Member, IEEE,* Anil Yesilkaya, *Student Member, IEEE,* Majid Safari, *Member, IEEE,* and Harald Haas, *Fellow, IEEE*

***Abstract*—A novel modulation scheme for an indoor optical wireless communication (OWC) system referred to as generalized time slot index modulation (GTIM) is proposed for single-carrier frequency domain equalization (SC-FDE) systems. This scheme is further referred to as SC-GTIM. In SC-GTIM, information bits are flexibly encoded onto both the amplitudes and positions of pulses. A set partitioning algorithm is proposed to construct a codebook for the SC-GTIM system. In this paper, SC-GTIM will be compared with the conventional pulse amplitude modulation-based SC-FDE (SC-PAM) and time slot index modulation-based SC-FDE (SC-TIM). By considering a multipath optical wireless channel and the limited dynamic range of a light emitting diode (LED), a considerable bit error ratio (BER) gain can be achieved by SC-GTIM. It is concluded that SC-GTIM is a promising technique for low to medium spectral efficiency transmission and uplink schemes.**

***Index Terms*—PAM, frequency domain equalization, index modulation, optical wireless communication.**

I. Introduction

THE recent forecasts in 2016 show that 60% of mobile data traffic is offloaded to a fixed network, e.g., WiFi or femtocell [2]. An exponentially growing number of mobile devices, followed by the ever-increasing mobile data traffic, is predicted to increase sevenfold in 2021. Moreover, cutting edge technologies, namely augmented/virtual reality (AR/VR), internet-of-things (IoT), massive machine-type communications (MMTC) and ultra high definition video/gaming applications create a data greedy ecosystem. This progressive demand will rapidly drain the capabilities of the existing radio communication technologies. To cope with this issue, higher frequencies (above 6 GHz) spectra are being utilized, such as milimeter wave (30 GHz to 300 GHz) [3], terahertz (300 GHz to 3 THz) [4] and optical wireless communications (OWC) (10 THz to 1 PHz) [5]. Specifically, OWC can enable a high area spectral efficiency that can further boost the network capacity [6], [7]. Furthermore, OWC offers an unlicensed and very wide spectra which opens abundant opportunities for wireless systems to meet future mobile data traffic demands [7].

Inspired from spatial modulation (SM) [8], [9], which encodes both constellation symbols and transmit antenna index, the term index modulation (IM) is first introduced in [10]. Instead of the transmit antenna index, subcarriers are used in [10]. This method is referred to as subcarrier-IM orthogonal frequency division multiplexing (OFDM). These transmit entities, namely transmit index (space domain) and subcarrier index (frequency domain), can be extended to other domains such as time domain [11], [12] or combinations of them [13], [14]. In fact, IM is not only limited to these domains, and could, for example, include orbital angular momentum (OAM) [15]. Recent survey papers in [16]–[18] summarize that IM appears to be a potential candidate for the future wireless communication systems due to its spectral and energy efficiency as well as lower hardware complexity. These advantages can also be adopted to OWC, and this paper aims to focus on this topic.

In this paper, we specifically focus on the application of time-domain IM, namely time slot IM (TIM), to intensity modulation and direct detection (IM/DD)-based OWC. We base our work on the recent application of TIM to a single-carrier frequency domain equalization (SCFDE)-based system as discussed in [11]. In [11], both time slots and constellation symbols are simultaneously encoded at the transmitter side. In the context of single carrier (SC) transmissions in IM/DD-based OWC, SCFDE systems have been studied in [19], [20]. It is concluded that the SCFDE systems offer lower computational complexity and lower peak-to-average power ratio (PAPR) compared to OFDM-based and carrierless amplitude and phase (CAP) systems. To the best of our knowledge, both limitations and advantages of TIM to SCFDE systems in OWC have not been investigated in detail.

Contribution: First, we show that the advantages of applying TIM to pulse-amplitude modulation (PAM)-SCFDE with linear dynamic range of light emitting diode (LED) are very limited. These limitations are mainly due to the constraint of choosing a fixed number of active time slots, which can cause the minimum Euclidean distance of the constellation symbols is smaller than that of the conventional system. Then, a novel TIM, namely generalized TIM (GTIM), which removes the constraint and allows arbitrary number of active time slots, is proposed. In addition, we also propose a set partitioning algorithm to design a good codebook which maximizes both Hamming and Euclidean distances. Consequently, the error performance of the proposed system shows a significant gain

Manuscript received Jul 30, 2019; revised Jan 30, 2020; accepted March 1, 2020. A. Purwita acknowledges the financial support from Indonesian Endowment Fund for Education (LPDP). A. Yesilkaya acknowledges the financial support from Zodiac Inflight Innovations (TriaGnoSys GmbH). H. Haas acknowledges financial support from the Engineering and Physical Sciences Research Council (EPSRC) under the Established Career Fellowship grant no. EP/R007101/1 as well as the Wolfson Foundation and the Royal Society. H. Haas and M. Safari acknowledge the financial support from EPSRC under grant no. EP/S016570/1 'Terabit Bidirectional Multi-user Optical Wireless System (TOWS) for 6G LiFi'.

The authors are with School of Engineering, Institute for Digital Communications, LiFi R&D Centre, The University of Edinburgh, Edinburgh EH9 3JL, U.K. (e-mail: {a.purwita, a.yesilkaya, majid.safari, h.haas}@ed.ac.uk).

This work has been partially presented in the IEEE PIMRC 2019 [1].

compared to both TIM-based and conventional systems.

A. Related Works

In the context of OWC with intensity modulation and direct detection, TIM can be interpreted as a hybrid PAM and pulse-position modulation (PPM) system from the perspective of IM due to the real and positivity constraints of the transmitted signal. This fact is also stated in [17]. In order to increase the spectral efficiency, PAM and PPM are merged and proposed in [21] for optical fibre communications. After that, several works have been published on the generalization of time domain pulses. In [22], an attempt to generalize conventional PPM is made. Unlike conventional PPM, two pulses are activated in a single block. A year after, a bandwidth efficient generalization of PPM, namely multiple PPM (MPPM) is proposed in [23] for optical communications. In 2004, the combination of PAM and PPM are used for ultra wideband systems [24], which is referred to as PPAM. The constructions of signal sets of PPAM are provided in [25], which is based on Euclidean distances and in [26], which uses the set partitioning algorithm for a trellis coded modulation [27]. Multiple PPAM (MPAPM) for OWC is briefly discussed in [28]. Combinations of TIM-based systems and other transmission entities, e.g., transmit antennas, are presented in [13], [14], [29]. In [11], single-carrier index modulation (SCIM) is proposed where only time slot entity is used without combining with other entities. In this paper, the advantages and limitations of the application of TIM in OWC systems are investigated. To the best of our knowledge, a similar study has not been presented yet.

The remainder of this paper is organized as follows. A system model for the PAM-SCFDE is provided in Section II. TIM and GTIM will be discussed in Section III. The proposed construction method for GTIM is given in Section IV. In Section V, simulation and analytical results are provided. Section VI concludes this paper.

Notation: A boldface, lower case letter denotes a vector, and a bold face, upper case letter denotes a matrix. The expected value and floor operations are denoted by $\mathbb{E}[\cdot]$ and $\lfloor\cdot\rfloor$, respectively. The superscripts T or H denote a transpose and a Hermitian transpose of a vector or a matrix, respectively. The tail distribution function of a standard normal distribution is denoted by $Q(\cdot)$.

II. System Model

A. Transmitter and Receiver Models

A block-based transmission system with a cyclic prefix (CP) and N-point discrete Fourier transform (DFT) is used in this paper as depicted in Fig. 1. The B_{t}-bit binary vector $\mathbf{b}$ is partitioned into L sub-blocks, i.e., $\mathbf{b} = [\mathbf{b}_0^{\mathrm{T}}, \mathbf{b}_1^{\mathrm{T}}, \cdots, \mathbf{b}_{L-1}^{\mathrm{T}}]^{\mathrm{T}}$, such that $J = N/L$, where J is a time slot length. The length of each vector $\mathbf{b}_l$ becomes, $B = B_{\mathrm{t}}/L$ bits. Then, each $\mathbf{b}_l$ is mapped onto a $J-$length symbol vector $\mathbf{s}_l = \left[s_{l,0}, s_{l,1}, \cdots, s_{l,J-1}\right]^{\mathrm{T}}$ by a one-to-one mapping function $f_{\mathcal{S}}$ according to a set $\mathcal{S} \in \left\{\mathcal{S}^{\mathrm{PAM}}, \mathcal{S}^{\mathrm{TIM}}, \mathcal{S}^{\mathrm{GTIM}}\right\}$ which denotes the codebooks of the unipolar SC-PAM, SC-TIM and SC-GTIM, respectively. Note that throughout this paper, SC-PAM refers to PAM-SCFDE [19], SC-TIM refers to PAM-based SCIM, and the proposed GTIM will be referred to as SC-GTIM. Finally, the transmitted symbol vector is defined as $\mathbf{s} = \left[\mathbf{s}_0^{\mathrm{T}}, \mathbf{s}_1^{\mathrm{T}}, \cdots, \mathbf{s}_{L-1}^{\mathrm{T}}\right]^{\mathrm{T}}$ whose length is N symbols.

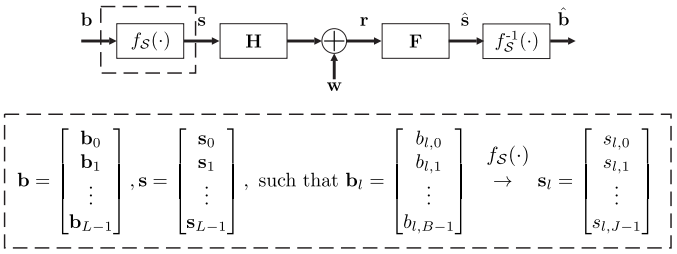

Fig. 1. A system model of PAM with block transmission and CP.

For a unipolar M-PAM, the elements of the symbol vectors are chosen from a set of symbols, which is defined as:

$$\mathcal{P}_M = \left\{ I_{\mathrm{a}} + \frac{I_{\mathrm{b}} - I_{\mathrm{a}}}{M-1} i \;\middle|\; i \in \{0, 1, \cdots, M-1\}, [I_{\mathrm{a}}, I_{\mathrm{b}}] \subset \mathbb{R}^+ \right\}.$$

Note that the constellation set $\mathcal{P}_M$ is defined such that the linear dynamic range of an LED, which is defined as $[I_{\mathrm{a}}, I_{\mathrm{b}}]$, is incorporated. Intuitively, the symbol $s_{l,j} \in \mathcal{P}_M$ models the driving current of an LED. Note that $[I_{\mathrm{a}}, I_{\mathrm{b}}]$ is assumed to be strictly positive. In practice, this is achieved by adding a DC bias.

Let η be the *normalized spectral efficiency* in bits per symbol, and it is defined as:

$$\eta \triangleq \frac{B}{J} \quad \text{(bits/symbol)}. \tag{1}$$

Note that the spectral efficiency of a block transmission in bps/Hz with PAM and the CP length of L_{cp} is [30, p. 226]:

$$R = \frac{N}{N + L_{\mathrm{cp}}} 2\eta \quad \text{(bps/Hz)}, \tag{2}$$

where $N/(N + L_{\mathrm{cp}})$ is the bandwidth penalty due to the CP.

For a block transmission with SC-PAM, the transmitted symbol vectors are chosen from the set $\mathcal{S}^{\mathrm{PAM}}$ which is defined as:

$$\mathcal{S}^{\mathrm{PAM}} = \left\{ \mathbf{s}_l = [s_{l,0}, s_{l,1}, \cdots, s_{l,J-1}]^{\mathrm{T}} \;\middle|\; s_{l,j} \in \mathcal{P}_M \right\},$$

where $\left|\mathcal{S}^{\mathrm{PAM}}\right| = 2^B$ is the cardinality of the set $\mathcal{S}^{\mathrm{PAM}}$. Typically, SC-PAM is defined with $J = 1$ and $s_l \in \mathcal{P}_M$ for $l = \{0, 1, 2, \cdots, L-1 = N-1\}$. For example, with $M = 2$ and $B = 1$, if $b_{l,0} = 0$, then $s_{l,0}$ is mapped to $s_{l,0} = I_{\mathrm{a}}$. Otherwise, $s_{l,0}$ is mapped to $s_{l,0} = I_{\mathrm{b}}$. Equivalently with $J = 2$, the set $\mathcal{S}^{\mathrm{PAM}}$ can also be expressed as:

$$\mathcal{S}^{\mathrm{PAM}} = \left\{ \underset{\substack{b_{l,0}=[0] \\ b_{l,1}=[0]}}{\begin{bmatrix} I_{\mathrm{a}} \\ I_{\mathrm{a}} \end{bmatrix}}, \underset{\substack{b_{l,0}=[1] \\ b_{l,1}=[0]}}{\begin{bmatrix} I_{\mathrm{b}} \\ I_{\mathrm{a}} \end{bmatrix}}, \underset{\substack{b_{l,0}=[0] \\ b_{l,1}=[1]}}{\begin{bmatrix} I_{\mathrm{a}} \\ I_{\mathrm{b}} \end{bmatrix}}, \underset{\substack{b_{l,0}=[1] \\ b_{l,1}=[1]}}{\begin{bmatrix} I_{\mathrm{b}} \\ I_{\mathrm{b}} \end{bmatrix}} \right\}. \tag{3}$$

Notice that the mapping remains the same as in the case with $J = 1$. This representation will be used to relate SC-PAM to SC-TIM and SC-GTIM. For SC-PAM, the Gray code is always used to ensure the optimality in the sense of error probability

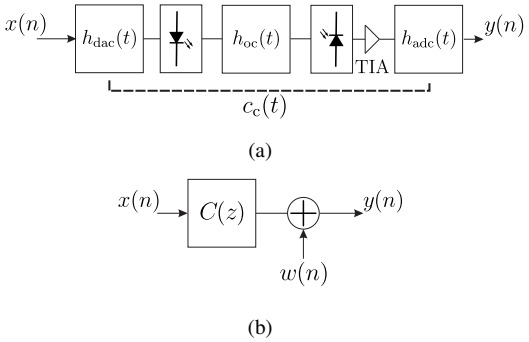

Fig. 2. (a) A continuous-time channel model after the parallel-to-serial conversion and before the serial-to-parallel conversion, and (b) a discrete-time equivalent channel model.

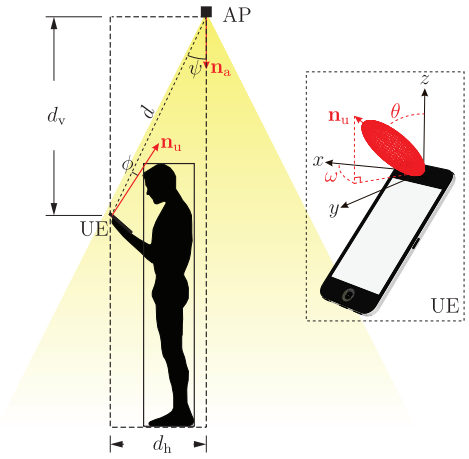

Fig. 3. A geometric model for the optical channel.

[31]. For a unit energy transmit pulse, the energy per symbol for the SC-PAM is denoted as:

$$E_{\mathrm{s,PAM}} = \frac{1}{|\mathcal{P}_M|}\sum_{s\in\mathcal{P}_M}|s|^2 = \frac{1}{6}\left(2\left(I_{\mathrm{a}}^2 + I_{\mathrm{a}}I_{\mathrm{b}} + I_{\mathrm{b}}^2\right) + \frac{(I_{\mathrm{b}}-I_{\mathrm{a}})^2}{M-1}\right), \tag{4}$$

where the second equality is obtained from sum of series formula. The energy per bit is denoted by $E_{\mathrm{b,PAM}} = E_{\mathrm{s,PAM}}/\eta$.

A discrete-time channel $c(n)$ is formed by sampling a continuous-time channel impulse response $c_{\mathrm{c}}(t)$ with a symbol rate R_{s}. The impulse response $c_{\mathrm{c}}(t)$ is the cascaded finite impulse response (FIR) filter that models a digital-to-analog converter (DAC), $h_{\mathrm{dac}}(t)$; LED, $h_{\mathrm{led}}(t)$; a frequency-selective wireless optical channel (WOC), $h_{\mathrm{oc}}(t)$; a photodiode (PD), $h_{\mathrm{pd}}(t)$; a transimpedance amplifier (TIA); and an analog-to-digital converter (ADC), $h_{\mathrm{adc}}(t)$, see Fig. 2. Note that $x(n)$ and $y(n)$ are the discrete-time transmitted and received symbols after the parallel-to-serial conversion and before the serial-to-parallel conversion, respectively. An additive white noise $w(n)$ with zero mean and variance σ_w^2 is used in this paper. This additive white noise represents both the thermal and shot noises that can be modeled as white, Gaussian, and signal-independent noise [32, p. 267].

B. Channel Model

As for the calculation of WOC, a frequency-domain approach proposed by Schulze [33] is used in this paper. The advantage of the frequency-domain approach is that infinite reflections can be taken into account. In addition, an arbitrarily-oriented device that is being held by a person is assumed, and a human body is modeled by a rectangular prism in the calculation of the WOC as in [34], [35].

The block-based transmission with PAM is applied for an uplink case due to a lower computational complexity and lower PAPR requirements at the transmitter side. Furthermore, it is assumed that the transmission is carried out over the infrared (IR) spectrum to avoid any visual discomfort for the users. An attenuation factor between the access point (AP) and the user equipment (UE), which is illustrated in Fig. 3, is defined as follows:

$$H = \frac{m+1}{2\pi}\cos^m(\phi)\frac{A_{\mathrm{AP}}\cos(\psi)}{d^2}v_{\mathrm{AP,UE}}(\mathrm{FoV}), \tag{5}$$

where m is the Lambertian index, A_{AP} denotes the AP photodetector area and ϕ is the radiance angle between the normal vector $\mathbf{n}_{\mathrm{u}}$ and the position of the AP. The incidence angle between the normal vector $\mathbf{n}_{\mathrm{a}}$ and the position of the UE is denoted by ψ. The orientations of an LED in the UE and a PD in the AP are shown by the unit normal vector $\mathbf{n}_{\mathrm{u}}$ and $\mathbf{n}_{\mathrm{a}}$, respectively. The distance between the UE and AP is denoted by d. A binary function $v_{\mathrm{AP,UE}}$ is the visibility factor of the link between an AP and UE, i.e., $v_{\mathrm{AP,UE}}$ is one if $-\pi/2 \le \phi \le \pi/2$ and zero otherwise. The visibility factor is also a function of the field-of-view (FoV) of a receiver. That is, $v_{\mathrm{AP,UE}}(\mathrm{FoV})$ is one if $0 \le \psi \le \mathrm{FoV} \le \pi/2$. The diffuse link can be calculated using a sum of products of (5) and the delay factor of reflecting surfaces, see [33] for more detailed information.

C. Equalization

With the CP length L_{cp} being equal or larger than the length of the channel taps, the discrete-time channel model can be denoted as:

$$C(z) = \sum_{n=0}^{L_{\mathrm{cp}}} c(n)z^{-n}. \tag{6}$$

The $N \times N$ channel matrix $\mathbf{H}$ is a circulant matrix whose first column is $\left[c(0), c(1), \ldots, c(L_{\mathrm{cp}}), \mathbf{0}\right]^{\mathrm{T}}$, where $N \ge L_{\mathrm{cp}}$. A circulant matrix can be diagonalized by using a normalized DFT matrix $\mathbf{W}$ as:

$$\mathbf{H} = \mathbf{W}^{\mathrm{H}}\mathbf{\Gamma}\mathbf{W},$$

where $\mathbf{\Gamma}$ is a $N \times N$ diagonal matrix whose diagonal entry is the N-point DFT of the channel tap $c(n)$. At the receiver side, the received symbol vectors $\mathbf{r}$ are equalized by a feedforward equalization matrix $\mathbf{F}$. Finally, the estimated symbol vectors $\hat{\mathbf{s}}$ are further processed to obtain an estimated bit stream of $\mathbf{b}$, which is denoted with $\hat{\mathbf{b}}$, by using the inverse of the mapping function $f_{\mathcal{S}}$, namely $f_{\mathcal{S}}^{-1}$.

A minimum mean square error (MMSE)-based filter is used in this paper. For a block transmission of PAM, it is shown in [36] that the optimal filter $\mathbf{F}$ can be written as:

$$\mathbf{F} = \mathbf{R_s}\mathbf{H}^{\mathrm{H}}\left(\mathbf{H}\mathbf{R_s}\mathbf{H}^{\mathrm{H}} + \mathbf{R_w}\right)^{-1}, \tag{7}$$

where $\mathbf{R_s}$ denotes the autocorrelation matrix of $\mathbf{s}$, i.e., $\mathbf{R_s} \triangleq \mathbb{E}\left[\mathbf{s}\mathbf{s}^{\mathrm{H}}\right]$. The same definition also applies to the autocorrelation matrix of the noise vector $\mathbf{w}$, i.e., $\mathbf{R_w} = \mathbb{E}\left[\mathbf{w}\mathbf{w}^{\mathrm{H}}\right] = \sigma_w^2\mathbf{I}$. A brute-force search is used to estimate the transmitted symbol, i.e.,:

$$\hat{\mathbf{s}}_l = \arg\min_{\mathbf{s}_l \in \mathcal{S}^{\mathrm{TIM}}} ||\hat{\mathbf{s}}_l - \mathbf{s}_l||. \tag{8}$$

Then, $\mathbf{b}_l$ is estimated by $\hat{\mathbf{b}}_l = f^{-1}_{\mathcal{S}^{\mathrm{TIM}}}\left(\hat{\mathbf{s}}_l\right)$.

III. Time Slot Index Modulation

For readability purposes, TIM for SC-FDE will be first explained based on [11]. Then, it is followed by the generalization of the SC-TIM, namely SC-GTIM. To apply an IM to SC-PAM, an additional symbol is required to denote that a transmission entity is inactive. In our case, that transmission entity is a time slot. The additional symbol is denoted as I_0. Therefore, by applying IM to SC-PAM, a symbol $s_{l,j}$ is now $s_{l,j} \in \{\mathcal{P}_M, \{I_0\}\}$. The same argument is also used in [37, p. 736]. In the IM literature [16], [17], [37], I_0 is typically chosen to be 0. In this paper, we assume a general case where $I_0 \in \{0, I_{\mathrm{a}} - \epsilon\}$, for a small positive value ϵ. A reason to choose $I_0 = I_{\mathrm{a}} - \epsilon$ is to minimize the effect of the rapid switching problem, which decreases the lifetime of an LED, if I_0 is chosen to be 0.

A. Single-Carrier Time Slot Index Modulation (SC-TIM)

In SC-TIM, the B-bit vector $\mathbf{b}_l$ contains a B_1-bit and a B_2-bit binary vectors, i.e., $B = B_1 + B_2$. A B_1-bit binary vector is used to modulate the index of the active time slots. Note that B_1 is defined such that K out of J are chosen from the set $\mathcal{P}_M$, and the others are set to be I_0. It is also worth noting that K out of J can be interpreted as choosing K out of J *time slots* to be active. A B_2-bit binary vector is used to modulate the $M-$PAM symbols from $\mathcal{P}_M$. Therefore, B_1 and B_2 can be calculated as:

$$B_1 = \left\lfloor \log_2 \binom{J}{K} \right\rfloor, \text{ and } B_2 = K \log_2 M. \tag{9}$$

For example, with $K = 1$, $J = 2$ and $\mathcal{P}_2 = \{I_{\mathrm{a}}, I_{\mathrm{b}}\}$, we have the possible transmitted symbol $\mathbf{s}_l \in \mathcal{S}^{\mathrm{TIM}}$, such that the mapping set $\mathcal{S}^{\mathrm{TIM}}$ is:

$$\mathcal{S}^{\mathrm{TIM}} = \left\{ \underset{\substack{b_{l,0}=[0]\\ b_{l,1}=[0]}}{\begin{bmatrix} I_0 \\ I_{\mathrm{a}} \end{bmatrix}}, \underset{\substack{b_{l,0}=[1]\\ b_{l,1}=[0]}}{\begin{bmatrix} I_0 \\ I_{\mathrm{b}} \end{bmatrix}}, \underset{\substack{b_{l,0}=[0]\\ b_{l,1}=[1]}}{\begin{bmatrix} I_{\mathrm{a}} \\ I_0 \end{bmatrix}}, \underset{\substack{b_{l,0}=[1]\\ b_{l,1}=[1]}}{\begin{bmatrix} I_{\mathrm{b}} \\ I_0 \end{bmatrix}} \right\}. \tag{10}$$

In this case, $b_{l,1} = 0$ denotes the first time slot as inactive, while $b_{l,1} = 1$ denotes the second time slot as inactive. In addition, $b_{l,0} = 0$ denotes that the PAM constellation symbol I_{a} is chosen. Otherwise, the PAM constellation symbol I_{b} is chosen. A working principle of (10) is shown in Fig. 4. Following the notation in Section II, suppose the binary input vector is $\mathbf{b} = [1,0,1,1,0,1,0,0,1,0]^{\mathrm{T}}$ and $L = 5$, then we have $\mathbf{b}_0 = [b_{0,0}, b_{0,1}]^{\mathrm{T}} = [1,0]^{\mathrm{T}}$, $\mathbf{b}_1 = [b_{1,0}, b_{1,1}]^{\mathrm{T}} = [1,1]^{\mathrm{T}}$, etc. Based on (10), $[1,0]^{\mathrm{T}}$ maps to $[I_0, I_{\mathrm{b}}]^{\mathrm{T}}$, and $[1,1]^{\mathrm{T}}$ maps to $[I_{\mathrm{b}}, I_0]^{\mathrm{T}}$ consecutively.

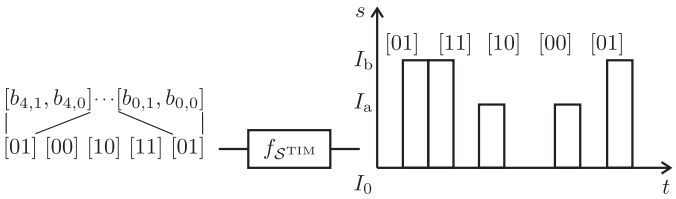

Fig. 4. The working principle of $f_{\mathcal{S}^{\mathrm{SCTIM}}}$ with (10).

Compared to the energy per symbol of the SC-PAM in (4), it is generally harder to obtain a compact expression for $\mathbf{R_s}$. The naive way is (i) to list all possible combinations of alphabets $\mathbf{s}\mathbf{s}^{\mathrm{H}}$; (ii) count the frequency of each element of the alphabet for given parameters M, K and J; and (iii) calculate $\mathbf{R_s} = \mathbb{E}\left[\mathbf{s}\mathbf{s}^{\mathrm{H}}\right]$ by taking the expectation value of all possible combinations. However, for $K = 1$ and $I_0 = 0$, $\mathbf{R_s}^{\mathrm{TIM},K=1}$ can be found as shown in (11). The constants p and q can be calculated as:

$$p = \frac{1}{2^B}\sum_{s\in\mathcal{P}_M}|s|^2 = \frac{\left(\left(I_{\mathrm{a}}^2 + I_{\mathrm{b}}^2\right)(2M-1) + 2I_{\mathrm{a}}I_{\mathrm{b}}(M-2)\right)}{3\left(1-\frac{1}{M}\right)2^{(B+1)}},$$

$$q = \frac{1}{2^J 2^M}\sum_{x\in\mathcal{P}_M}\sum_{y\in\mathcal{P}_M} xy = M^2(I_{\mathrm{a}} + I_{\mathrm{b}})^2 2^{-(J+M+2)},$$

where sum of series formula is used to obtain these expressions. It is worth noting that $\mathbf{R_s}^{\mathrm{TIM},K=1}$ is not a circulant matrix. This is an example of a scenario when the simple single-tap equalization cannot always be performed by a PAM-based SC-TIM. In this case, the PAM-based SC-TIM has a higher computational complexity.

Note that p is also the average energy per symbol for the PAM-based SC-TIM which is lower than that without TIM, i.e., $E_{\mathrm{s,TIM}} = p \leq E_{\mathrm{s,PAM}}$. Typically, IM has lower transmitted energy due to the value of the additional symbol, i.e., I_0, that is usually 0. However, in terms of PAPR, the PAM-based SC-TIM has a larger PAPR as the peak value of $\mathbf{s}$ is still I_{b}, while the average energy is lower. It is worth noting that the increase in PAPR does not occur for other IM systems such as OFDM-IM, where the PAPR is the same as the conventional OFDM system, see Fig. 4 in [17].

For an IM scheme, an average pairwise-error probability (PEP) over all possible pairs of symbols is typically used as an upper bound. The average BER is upper bounded by the average PEP (APEP), that is,:

$$P_{\mathrm{b}} \leq \frac{1}{B2^B}\sum_{\mathbf{s}_i\in\mathcal{S}^{\mathrm{TIM}}}\sum_{\substack{\mathbf{s}_j\in\mathcal{S}^{\mathrm{TIM}}\\ \mathbf{s}_j\neq\mathbf{s}_i}} d_{\mathrm{H}}(\mathbf{s}_i,\mathbf{s}_j)P\left(\mathbf{s}_i\rightarrow\mathbf{s}_j\right) = \mathrm{APEP}. \tag{12}$$

$$\mathbf{R}_{\mathbf{s}}{}^{\mathrm{TIM},K=1}_{N\times N} = \begin{bmatrix} \begin{bmatrix} p & 0 & \cdots & 0 \\ 0 & p & \cdots & 0 \\ \vdots & \vdots & \ddots & \vdots \\ 0 & 0 & \cdots & p \end{bmatrix}_{J\times J} & \begin{bmatrix} q & q & \cdots & q \\ q & q & \cdots & q \\ \vdots & \vdots & \ddots & \vdots \\ q & q & \cdots & q \end{bmatrix}_{J\times J} & \cdots & \begin{bmatrix} q & q & \cdots & q \\ q & q & \cdots & q \\ \vdots & \vdots & \ddots & \vdots \\ q & q & \cdots & q \end{bmatrix}_{J\times J} \\ \begin{bmatrix} q & q & \cdots & q \\ q & q & \cdots & q \\ \vdots & \vdots & \ddots & \vdots \\ q & q & \cdots & q \end{bmatrix}_{J\times J} & \begin{bmatrix} p & 0 & \cdots & 0 \\ 0 & p & \cdots & 0 \\ \vdots & \vdots & \ddots & \vdots \\ 0 & 0 & \cdots & p \end{bmatrix}_{J\times J} & \cdots & \begin{bmatrix} q & q & \cdots & q \\ q & q & \cdots & q \\ \vdots & \vdots & \ddots & \vdots \\ q & q & \cdots & q \end{bmatrix}_{J\times J} \\ \vdots & \vdots & \ddots & \vdots \\ \begin{bmatrix} q & q & \cdots & q \\ q & q & \cdots & q \\ \vdots & \vdots & \ddots & \vdots \\ q & q & \cdots & q \end{bmatrix}_{J\times J} & \begin{bmatrix} q & q & \cdots & q \\ q & q & \cdots & q \\ \vdots & \vdots & \ddots & \vdots \\ q & q & \cdots & q \end{bmatrix}_{J\times J} & \cdots & \begin{bmatrix} p & 0 & \cdots & 0 \\ 0 & p & \cdots & 0 \\ \vdots & \vdots & \ddots & \vdots \\ 0 & 0 & \cdots & p \end{bmatrix}_{J\times J} \end{bmatrix} \tag{11}$$

A Hamming distance between the bits associated with both $\mathbf{s}_i$ and $\mathbf{s}_j$ is denoted by $d_{\mathrm{H}}(\mathbf{s}_i, \mathbf{s}_j)$. The PEP is defined as:

$$P\left(\mathbf{s}_i \to \mathbf{s}_j\right) = Q\left(\frac{d_{\mathrm{E}}(\mathbf{s}_i, \mathbf{s}_j)}{2\sqrt{\sigma_{\mathbf{e}}^2}}\right), \tag{13}$$

where $d_{\mathrm{E}}(\mathbf{s}_i, \mathbf{s}_j) = ||\mathbf{s}_i - \mathbf{s}_j||$ denotes the Euclidean distance between $\mathbf{s}_i$ and $\mathbf{s}_j$. The autocorrelation matrix of the error vector $\mathbf{e} = \hat{\mathbf{s}} - \mathbf{s}$ is defined as:

$$\mathbf{R}_{\mathbf{e}} \triangleq \mathrm{E}\left\{\mathbf{e}\mathbf{e}^{\mathrm{H}}\right\} = \left(\mathbf{R}_{\mathbf{s}}{}^{-1} + \mathbf{H}^{\mathrm{H}}\mathbf{R}_{\mathbf{w}}{}^{-1}\mathbf{H}\right)^{-1}, \tag{14}$$

where the Woodbury identity is used, see [36]. Let the average noise power of $\mathbf{e}$ be $\sigma_{\mathbf{e}}^2$, which is defined as:

$$\sigma_{\mathbf{e}}^2 \triangleq \mathrm{tr}\left(\mathbf{R}_{\mathbf{e}}\right)/N.$$

For the SC-PAM, instead of using the upper bound in (12), a good approximation can be obtained as follows:

$$P_{\mathrm{b,PAM}} \approx \frac{1}{N}\sum_{i=0}^{N-1} \frac{2}{\log_2 M}\left(1 - \frac{1}{M}\right) Q\left(f(I_{\mathrm{a}}, I_{\mathrm{b}}, \beta_i)\right), \tag{15}$$

$$f(I_{\mathrm{a}}, I_{\mathrm{b}}, \beta_i) = \sqrt{\frac{1.5(I_{\mathrm{b}} - I_{\mathrm{a}})^2 \log_2(M)\beta_i}{(M-1)^2\left(2\left(I_{\mathrm{a}}^2 + I_{\mathrm{a}}I_{\mathrm{b}} + I_{\mathrm{b}}^2\right) + \frac{(I_{\mathrm{b}} - I_{\mathrm{a}})^2}{M-1}\right)}},$$

where the Gray code is assumed and $\beta_i = E_{\mathrm{b,PAM}}/[\mathbf{R}_{\mathbf{e}}]_i$. It is assumed in (15) that the error vector $\mathbf{e}$ coming from both the noise $\mathbf{w}$ and the remaining intersymbol interference (ISI) is approximated by a Gaussian distribution [38].

B. Single-Carrier Generalized Time Slot Index Modulation (SC-GTIM)

The main difference between SC-TIM and SC-GTIM is that K does not have to be fixed in SC-GTIM. To compare it with (10), we have, for example,:

$$\mathcal{S}^{\mathrm{GTIM}} = \left\{ \underset{b_{l,0}=[0]\ b_{l,1}=[0]}{\begin{bmatrix} I_0 \\ I_0 \end{bmatrix}}, \underset{b_{l,0}=[1]\ b_{l,1}=[0]}{\begin{bmatrix} I_{\mathrm{b}} \\ I_0 \end{bmatrix}}, \underset{b_{l,0}=[0]\ b_{l,1}=[1]}{\begin{bmatrix} I_0 \\ I_{\mathrm{b}} \end{bmatrix}}, \underset{b_{l,0}=[1]\ b_{l,1}=[1]}{\begin{bmatrix} I_{\mathrm{b}} \\ I_{\mathrm{b}} \end{bmatrix}} \right\}, \tag{16}$$

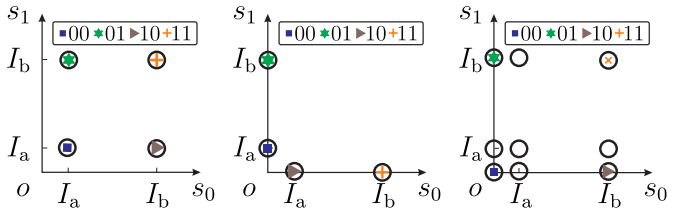

(a) SC-PAM (3) (b) SC-TIM (10) (c) SC-GTIM (16)

Fig. 5. Vector representations: (a) SC-PAM with $M = 2$ and the Gray code and without IM ($\eta = 1$), (b) SC-TIM with $K = 1$ and $J = 2$ ($\eta = 1$) and (c) SC-GTIM with $J = 2$ ($\eta = 1$). The circle markers show the symbols that can be chosen and labeled with binary vectors. The other markers show the chosen symbols.

where the number of bits in SC-GTIM is defined as $B = \log_2|\mathcal{S}^{\mathrm{GTIM}}|$. Notice that K is not fixed for all elements of $\mathcal{S}^{\mathrm{GTIM}}$ in the above example. In addition, SC-GTIM in (16) reduces to on-off keying (OOK) with return-to-zero pulse or PPM, which is known to achieve the Shannon capacity in low spectral efficiency regions [39]. It is worth mentioning that SC-TIM cannot be reduced to OOK as SC-TIM is constrained by (9), which shows less flexibility compared to SC-GTIM.

To illustrate the set $\mathcal{S}^{\mathrm{GTIM}}$ based on (16) and compare it with other examples in (3) and (10), the vector representations of $\left[s_{l,0}, s_{l,1}, \cdots, s_{l,J-1}\right]^{\mathrm{T}}$ are illustrated in Fig. 5. The point o_{I_0} is the shifted origin with respect to I_0. e.g., in $\mathbb{R}^2$, o_{I_0} is (I_0, I_0). The index l is omitted as it is not relevant. Note that a directed vector that starts from o_{I_0} is used. Fig. 5 uses circles to show all possible $\mathbf{s}_l$ that can be chosen and the directed vectors with markers to show the chosen $\mathbf{s}_l$. In this way, we have a classic constellation diagram representation. Fig. 5(c) clearly illustrates a more flexible constellation design of SC-GTIM compared to the others. If this can be cultivated fully, a significant performance gain can be achieved.

We now compare SC-GTIM with SC-TIM in (10). It is obvious to see that the BER of SC-TIM with $\mathcal{S}^{\mathrm{TIM}}$ expressed in (10) will be limited by the vectors $[I_0, I_{\mathrm{a}}]^{\mathrm{T}}$ and $[I_{\mathrm{a}}, I_0]^{\mathrm{T}}$ if $|I_{\mathrm{a}} - I_0| < |I_{\mathrm{b}} - I_{\mathrm{a}}|$. Consequently, the BER of SC-TIM is worse than that of the conventional SC-PAM. In this case, a codebook

that has more possible constellation points is required. This is where SC-GTIM has the advantage by means of freeing the number of active time slots.

A collection of possible codewords $\mathcal{S}^{\mathrm{s}}$ is defined as:

$$\mathcal{S}^{\mathrm{s}} = \left\{ \mathbf{s}_l = [s_{l,0}, s_{l,1}, \cdots, s_{l,J-1}]^{\mathrm{T}} \middle| \; s_{l,j} \in \{\mathcal{P}_M, \{I_0\}\} \right\}. \quad (17)$$

The indexing and grouping of all possible $[s_{l,0}, s_{l,1}, \cdots, s_{l,J-1}]^{\mathrm{T}} \in \mathcal{S}^{\mathrm{GTIM}} \subseteq \mathcal{S}^{\mathrm{s}}$ will affect the BER. There are:

$$G = \frac{(M+1)^J!}{\left((M+1)^J - 2^B\right)!} \quad (18)$$

ways of indexing and grouping in the construction of the set $\mathcal{S}^{\mathrm{GTIM}}$. Based on (13) and the upper bound in (12), the design problem can be formulated as:

$$\begin{aligned} \underset{\mathcal{S}^{\mathrm{GTIM}}}{\arg\max} \quad & C = \sum_{\mathbf{s}_i \in \mathcal{S}^{\mathrm{GTIM}}} \sum_{\substack{\mathbf{s}_j \in \mathcal{S}^{\mathrm{GTIM}} \\ \mathbf{s}_j \neq \mathbf{s}_i}} d_{\mathrm{H}}(\mathbf{s}_i, \mathbf{s}_j) d_{\mathrm{E}}(\mathbf{s}_i, \mathbf{s}_j) \quad (19) \\ \text{subject to:} \quad & |\mathcal{S}^{\mathrm{GTIM}}| = 2^B. \end{aligned}$$

The problem in (19) can be seen as the problem of choosing 2^B active vectors in $\left[s_{l,0}, s_{l,1}, \cdots, s_{l,J-1}\right]^{\mathrm{T}}$ and labeling them with a B-bit vector. To be more specific, the goal is to label a vector such that it has both large Hamming and Euclidean distances. As (19) is a combinatoric problem which has G many possible combinations, a meta-heuristic solution for a permutation-based combinatorial optimization problem can be used. However, it will be shown in the next section that a simpler way can be applied by using the knowledge of the Gray encoding.

C. Spectral Efficiency Comparison for Different Time Slot Length J

In this subsection, the normalized spectral efficiencies in bits per symbol of the conventional SC-PAM, SC-TIM and SC-GTIM are compared, see (2) for a conversion to the unit bps/Hz. Specifically, we are interested in the maximum achievable η given $M \geq 2$ and different J. Notice that it will be straightforward for both SC-PAM and SC-GTIM, but it is not the case for SC-TIM. For SC-TIM, the normalized spectral efficiency is defined as:

$$\eta_{\max}^{\mathrm{TIM}} = \max_{1 \leq K \leq J} \frac{\left\lfloor \log_2 \binom{J}{K} \right\rfloor + K \log_2 M}{J} \text{ and}$$

$$K^* = \inf \arg\max_{1 \leq K \leq J} \frac{\left\lfloor \log_2 \binom{J}{K} \right\rfloor + K \log_2 M}{J},$$

where inf denotes the infimum of a set. The infimum ensures that K^* is not J if there is another value except J. The closed form solutions of the above problem formulations are difficult to obtain due to the linear combination of the terms $\left\lfloor \log_2 \binom{J}{K} \right\rfloor$ and $K \log_2 M$.[1] Therefore, $\eta_{\max}^{\mathrm{TIM}}$ and K^* will be calculated numerically.

[1] If the term $K \log_2 M$ does not exist, then it is straightforward given that $\arg\max_K \binom{J}{K}$ is the nearest integer of $J/2$.

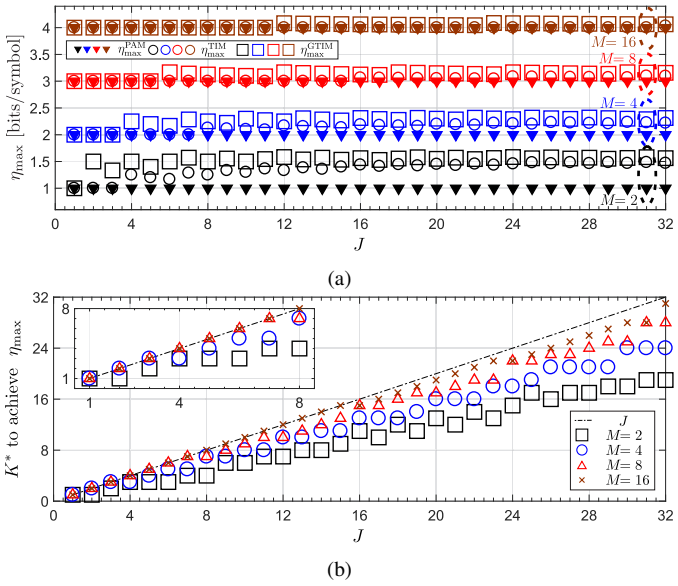

Fig. 6. (a) Maximum achievable η for SC-TIM, $\eta_{\max}^{\mathrm{TIM}}$, and (b) K optimal to achieve $\eta_{\max}^{\mathrm{TIM}}$, K^*.

As for the conventional SC-PAM, it can be readily obtained as $\eta_{\max}^{\mathrm{PAM}} = \log_2 M$. For SC-GTIM, given M and J, there are $(M+1)^J$ possible choices of vector $\mathbf{s}_l$, see (17). Therefore, the number of bits that can be transmitted for SC-GTIM is upper bounded by:

$$2^B \leq (M+1)^J.$$

Using the definition of η in (1) and the fact that B must be an integer, we have:

$$\eta_{\max}^{\mathrm{GTIM}} = \lfloor J \log_2(M+1) \rfloor / J.$$

Hence, $\eta_{\max}^{\mathrm{PAM}} \leq \eta_{\max}^{\mathrm{GTIM}}$. The numerical results for $\eta_{\max}$ of all systems are shown in Fig. 6(a). Therefore, we have $\eta_{\max}^{\mathrm{PAM}} \leq \eta_{\max}^{\mathrm{TIM}} \leq \eta_{\max}^{\mathrm{GTIM}}$. This shows the advantages of SC-GTIM in terms of spectral efficiency.

It is also interesting to discuss K^* as shown in Fig. 6(b). Based on (9), SC-TIM with $K = J$ reduces to SC-PAM. It means that when $K^* = J$, then SC-TIM cannot have a better spectral efficiency than that of SC-PAM. This illustrates the disadvantage of having a fixed number of active time slots.

IV. Construction of a Good Set $\mathcal{S}^{\mathrm{GTIM}}$

In this section, the construction of a good set $\mathcal{S}^{\mathrm{GTIM}}$ is provided. We start with a simple example in two dimensions (2-D), i.e., $J = 2$, and this is followed by an introduction of several necessary notations. Then, a more detailed algorithm is given next with more relevant examples having higher dimensions, i.e., $J > 2$.

A. Simple Example in 2-D (J = 2)

For a better enumeration and illustration, $\mathcal{P}_M$ is redefined as:

$$\mathcal{P}_M = \{m_0, m_1, \cdots, m_{M-1} | \; I_{\mathrm{a}} = m_0 < m_1 < \cdots < m_{M-1} = I_{\mathrm{b}}\},$$

Now, assume that a uniform M-PAM constellation is used, i.e., $|m_i - m_j| = c, \forall i \neq j \in \{0, 1, \cdots, M-1\}$ and a positive constant c. In this example, we use the following collection of possible codewords:

$$\mathcal{S}^{\mathrm{s}} = \left\{ \begin{bmatrix} I_0 \\ I_0 \end{bmatrix}, \begin{bmatrix} m_0 \\ I_0 \end{bmatrix}, \begin{bmatrix} m_1 \\ I_0 \end{bmatrix}, \begin{bmatrix} I_0 \\ m_0 \end{bmatrix}, \begin{bmatrix} m_0 \\ m_0 \end{bmatrix}, \begin{bmatrix} m_1 \\ m_0 \end{bmatrix}, \begin{bmatrix} I_0 \\ m_1 \end{bmatrix}, \begin{bmatrix} m_0 \\ m_1 \end{bmatrix}, \begin{bmatrix} m_1 \\ m_1 \end{bmatrix} \right\},$$

which represents the case where $M = 2$ and $J = 2$. Suppose that we define $B = 3$ bits, then we should pick $2^3 = 8$ of $|\mathcal{S}^{\mathrm{s}}| = 9$. Now that we have defined $\mathcal{S}^{\mathrm{s}}$, our design problem can be summarized as follows:

given: M, B, J

choose 2^B of $\mathbf{s}_l \in \mathcal{S}^{\mathrm{s}}$ and label them with binary vector

such that the 2^B chosen $\mathbf{s}_l$ have as large C (see (19)) as possible.

The basic operation of the construction algorithm is the set partitioning algorithm denoted by `SP`. The following are simple illustrations of the heuristic steps taken in the `SP` operation. Now, we discuss them in a high level. In the next subsection, these steps will be formalized and detailed.

1) The first step: Choose 2 sets of $\lfloor (M+1)^J/2 \rfloor = 4$ vectors of $\mathbf{s}_l$ such that the Euclidean distance of the average or center of mass of two sets are maximum. Then, label each set with a binary value and denote the sets with $\mathbb{P}_{b_0}^{M=2,\tilde{J}=2}$, where $b_0 \in \{0,1\}$ and $\tilde{J}$ is the number of elements of $\mathbf{s}_l$ which are taken into account. In this case, all elements of $\mathbf{s}_l$ are taken into account at once as $\tilde{J} = J$. A sample of the result is illustrated in Fig. 7(a). The chosen symbol vectors are shown by squares, and the cross marker shows the unchosen symbol vector. It is worth noting here that the elements in the set $\mathbb{P}_{b_0}^{2,2}$ will be labeled as $[b_0 XX]$, where $X \in \{0,1\}$ denotes a binary digit that is not assigned yet. That is, elements in $\mathbb{P}_1^{2,2}$ will be labeled as [100], [101], [110] or [111] in the final step.

2) The second step: Partition each $\mathbb{P}_{b_0}^{2,2}$ as in the first step. The outputs are now denoted as $\mathbb{P}_{b_0,b_1}^{2,2}$, where b_0 is followed by $b_1 \in \{0,1\}$ in the subscripts. Now, each set $\mathbb{P}_{b_0,b_1}^{2,2}$ contains two vectors. The binary mapping of $\mathbb{P}_{b_0,b_1}^{2,2}$ is carried out such that it forms the Gray mapping with its neighbors. For example:

$$\mathbb{P}_{1,0}^{2,2} = \left\{ \begin{bmatrix} I_0 \\ m_0 \end{bmatrix}, \begin{bmatrix} I_0 \\ m_1 \end{bmatrix} \right\} \text{ and } \mathbb{P}_{1,1}^{2,2} = \left\{ \begin{bmatrix} m_0 \\ m_1 \end{bmatrix}, \begin{bmatrix} m_1 \\ m_1 \end{bmatrix} \right\}$$

are neighbors to each other, and [10] and [11] forms the Gray mapping. A complete mapping is shown in Fig. 7(b).

3) The third step: As only 1 remaining bit needs to be assigned, the final step is to make sure that each element forms the Gray mapping with its neighbors. As depicted in Fig. 7(c), the final chosen constellation symbols and their mappings are denoted as:

$$\tilde{\mathbb{P}}^{2,2} = \left(\underset{000}{\begin{bmatrix} I_0 \\ I_0 \end{bmatrix}}, \underset{001}{\begin{bmatrix} m_0 \\ I_0 \end{bmatrix}}, \underset{010}{\begin{bmatrix} m_1 \\ m_0 \end{bmatrix}}, \underset{011}{\begin{bmatrix} m_1 \\ I_0 \end{bmatrix}}, \underset{100}{\begin{bmatrix} I_0 \\ m_0 \end{bmatrix}}, \underset{101}{\begin{bmatrix} I_0 \\ m_1 \end{bmatrix}}, \underset{110}{\begin{bmatrix} m_1 \\ m_1 \end{bmatrix}}, \underset{111}{\begin{bmatrix} m_0 \\ m_1 \end{bmatrix}} \right), \quad (20)$$

which can be interpreted that each vector corresponds to the binary vectors written below it.

B. Notations

The main goal of this subsection is to generalize the previous notations before formalizing the proposed algorithm for all J. We start by generalizing the notation $\mathbb{P}$. A set of $\tilde{J}$-length vectors whose elements are taken from $\{\mathcal{P}_M, \{I_0\}\}$ is defined as:

$$\mathbb{P}^{M,\tilde{J}} = \left\{ \mathbf{p} = \left[p_0, p_1, \cdots, p_{\tilde{J}-1} \right]^{\mathrm{T}} \right\}, \text{ where } p_j \in \{\mathcal{P}_M, \{I_0\}\}.$$

The set $\mathbb{P}^{M,\tilde{J}}$ can be partitioned into $\mathbb{P}^{M,\tilde{J}} = \mathbb{P}_{x_{B-1}}^{M,\tilde{J}} \cup \mathbb{P}_{y_{B-1}}^{M,\tilde{J}} \cup \mathbb{P}_{\mathrm{dc}}^{M,\tilde{J}}$, where $x_{B-1} \neq y_{B-1} \in \{0,1\}$ and they are disjointed from each other. The set $\mathbb{P}_{\mathrm{dc}}^{M,\tilde{J}}$ is a set that is not processed for the next step. With respect to our previous example, this set is labeled as a cross marker in Fig. 7(a). Now, a mean or 'center of mass' vector of a subset $\mathbb{P}_{x_{B-1}}^{M,\tilde{J}}$ is defined as:

$$\mathbf{d}_{\mathrm{S}}\left(\mathbb{P}_{x_{B-1}}^{M,\tilde{J}} \right) = \frac{1}{|\mathbb{P}_{x_{B-1}}^{M,\tilde{J}}|} \sum_{\mathbf{p} \in \mathbb{P}_{x_{B-1}}^{M,\tilde{J}}} \mathbf{p}, \quad (21)$$

which is used to measure the distance between two subsets of $\mathbb{P}^{M,\tilde{J}}$. The subset $\mathbb{P}_{x_B}^{M,\tilde{J}}$ can be further partitioned into $\mathbb{P}_{x_{B-1}}^{M,\tilde{J}} \supset \mathbb{P}_{x_{B-1},x_{B-2}}^{M,\tilde{J}} \cup \mathbb{P}_{x_{B-1},y_{B-2}}^{M,\tilde{J}}$. This partition can be done until the array $[x_{B-1}, x_{B-2}, \cdots, x_0]$ is obtained. The subset of $\mathbb{P}^{M,\tilde{J}}$ has a binary vector associated with it, for example with $B = 3$, $\mathbb{P}_{x_{B-1},x_{B-2},x_{B-3}}^{M,\tilde{J}}$ associates with a binary vector $[x_{B-1}, x_{B-2}, x_{B-3}]$.

An *ordered* set $\mathcal{B}_B$ is a collection of B-bit binary vectors that are arranged based on the Gray code, i.e.,:

$$\mathcal{B}_B = \left(\tilde{\mathbf{b}}_0, \tilde{\mathbf{b}}_1, \cdots, \tilde{\mathbf{b}}_{2^B-1} \right), \quad (22)$$

where $\tilde{\mathbf{b}}_i = \left[\tilde{b}_{i,0}, \tilde{b}_{i,1}, \cdots, \tilde{b}_{i,B-1} \right]^{\mathrm{T}}$, $\tilde{b}_{i,j} \in \{0,1\}$, $\tilde{b}_{i,0}$ and $\tilde{b}_{i,B-1}$ are the least significant bit (LSB) and the most significant bit (MSB), respectively. A common way to construct $\mathcal{B}_B$ is the iterative and mirroring method from $\mathcal{B}_{B-1}$ [31]. It follows that $\left[\tilde{b}_{i,0}, \tilde{b}_{i,1}, \cdots, \tilde{b}_{i,B-2} \right]^{\mathrm{T}} = \left[\tilde{b}_{2^B-1-i,0}, \tilde{b}_{2^B-1-i,1}, \cdots, \tilde{b}_{2^B-1-i,B-2} \right]^{\mathrm{T}}$ for $0 \leq i \leq \left\lfloor \frac{2^B-1}{2} \right\rfloor$, see following examples:

$$\mathcal{B}_2 = \left(\begin{bmatrix} 0 \\ 0 \end{bmatrix}, \begin{bmatrix} 1 \\ 0 \end{bmatrix}, \begin{bmatrix} 1 \\ 1 \end{bmatrix}, \begin{bmatrix} 0 \\ 1 \end{bmatrix} \right), \text{ or}$$

$$\mathcal{B}_3 = \left(\begin{bmatrix} 0 \\ 0 \\ 0 \end{bmatrix}, \begin{bmatrix} 1 \\ 0 \\ 0 \end{bmatrix}, \begin{bmatrix} 1 \\ 1 \\ 0 \end{bmatrix}, \begin{bmatrix} 0 \\ 1 \\ 0 \end{bmatrix}, \begin{bmatrix} 0 \\ 1 \\ 1 \end{bmatrix}, \begin{bmatrix} 1 \\ 1 \\ 1 \end{bmatrix}, \begin{bmatrix} 1 \\ 0 \\ 1 \end{bmatrix}, \begin{bmatrix} 0 \\ 0 \\ 1 \end{bmatrix} \right).$$

This inspires us to do the construction of the set $\mathcal{S}^{\mathrm{GTIM}}$ by means of partitioning the set $\mathcal{B}_B$.[2] That is, the MSB can be assigned first by following the Gray code without worrying about the other bits. In fact, it can be shown that the bit mapping as shown in Fig. 7 follows the iterative method discussed in [31].

Generally for $J > 2$, we need a container set denoting the elements that have been chosen and labeled. Let the set $\mathcal{S}$ be

[2]Note that the name set partitioning is also used in [27], but ours is different in the terms of the method used to partition and label the set. In addition, the algorithm in [27] does not discuss a method on how to choose a set of constellation symbols whose cardinality is smaller than the set of all possible constellation symbols. Joint Euclidean-distance and Hamming-distance search is also not discussed in [27].

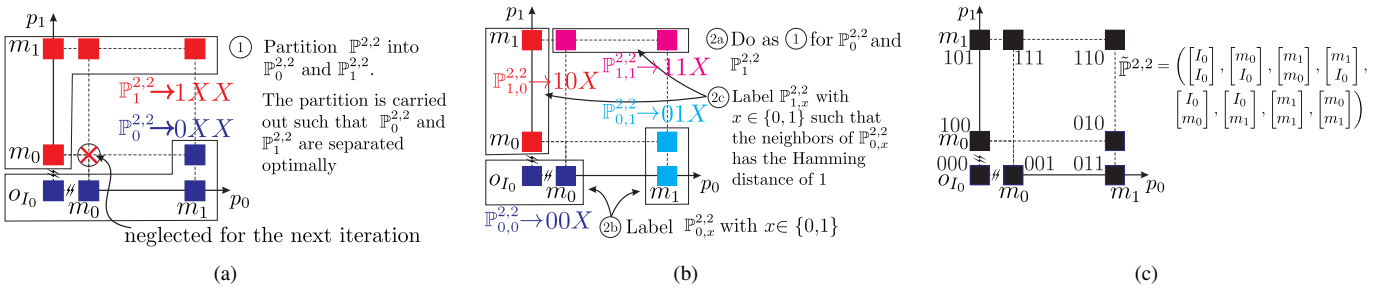

(a) (b) (c)

Fig. 7. (a) The first, (b) the second and (c) the third steps of the set partitioning algorithm.

an ordered set whose elements are indexed by the binary digit $\mathbf{b}_l$. As an example, see (3), where $\mathbf{b}_l = [b_{l,0}, b_{l,1}]^{\mathrm{T}} = [0,0]^{\mathrm{T}}$ indexes the 0^{th} element, and $[b_{l,0}, b_{l,1}]^{\mathrm{T}} = [1,0]^{\mathrm{T}}$ indexes the 1^{st} element. An ordered set $\mathbb{S}_{J-j}^{M}$ is defined as:

$$\mathbb{S}_{J-j}^{M} = \left(\begin{bmatrix} \mathbf{x} \\ s_{J-j} \\ \vdots \\ s_{J-2} \\ s_{J-1} \end{bmatrix} \right), \; s_{J-j} \in \{\mathcal{P}_M, \{I_0\}\}, \text{for } j \in \{0,1,\cdots,J-1\},$$

where $\mathbf{x}$ is the $(J-j)$-length column vector denoting the elements that *have not been defined yet*. In other words, $\mathbb{S}_{J-j}^{M}$ defines an ordered set where the $(J-j)^{\text{th}}$ to the $(J-1)^{\text{th}}$ elements *have been ordered and labeled*. For example with $M=3$, $B=6$, $J=3$, $j=1$ and:

$$\mathbb{S}_{3-1}^{3} = \left(\underset{00XXXX}{\begin{bmatrix} \mathbf{x} \\ I_0 \end{bmatrix}}, \underset{01XXXX}{\begin{bmatrix} \mathbf{x} \\ m_0 \end{bmatrix}}, \underset{10XXXX}{\begin{bmatrix} \mathbf{x} \\ m_2 \end{bmatrix}}, \underset{11XXXX}{\begin{bmatrix} \mathbf{x} \\ m_1 \end{bmatrix}} \right). \tag{23}$$

means that 2-length column vector $\mathbf{x}$ has not been defined; moreover, the 2^{nd} to the 3^{rd} elements have been ordered and labeled accordingly. The set $\mathcal{S}$ will be assigned as $\mathcal{S} = \mathbb{S}_0^M$ if all elements have been ordered and labeled. We use a convention that if no element has been assigned, then it is denoted by $\mathbb{S}_J^M$.

C. The Proposed Set Partitioning Algorithm

A complete pseudocode for the proposed set partitioning algorithm is given in algorithm 1 for a given M, B and J (or M, η and J). The main difference with the previous simple example is that for $J > 2$, the operation SP can be invoked multiple times. In addition, $\tilde{J}$ of J elements can be processed at once. The advantage of doing this is that it is more modular and more computationally efficient as the previously-defined mapping set can be reused.

In line 3, J_{b} denotes a parameter to control the number of steps such that they are upper bounded by $J - J_{\mathrm{b}} + 1$. The statement $J_{\mathrm{b}}\eta = \lfloor J_{\mathrm{b}}\eta \rfloor$ is used to avoid rounding the number of allocated bits to label $\mathbb{S}_0^M$. The variable J_{it} is used as a step size for the loop process in line 6. In line 6(h), B_{sp} denotes the number of bits required for labeling the set $\mathbb{S}_{J-(j-\tilde{J})}^{M}$ during the partitioning and labeling process, which is named as $\mathtt{SP}(\cdot)$ in line 6(i). Specifically, $\mathtt{SP}\left(\tilde{J}, B_{\mathrm{sp}}, \mathbb{S}_{J-(j-\tilde{J})}^{M}\right)$ reads so that the $\tilde{J}$ elements of the vector in the set $\mathbb{S}_{J-(j-\tilde{J})}^{M}$ will be labeled with B_{sp} bits, and the output is denoted as $\mathbb{S}_{J-j}^{M}$. The function SP will be formalized in the next subsection (at the first step of the first example). The steps detailed in lines 6(b-i) are repeatedly carried out until $j = J$. Therefore, if $J_{\mathrm{b}} = J$, then only 1 step is required. Generally, J_{b} can be interpreted as the number of elements of a vector in $\mathbb{S}^M$ that will be labeled at once in one step. Finally, the algorithm outputs $\mathcal{S}^{\mathrm{GTIM}}$ as $\mathcal{S}^{\mathrm{GTIM}} = \mathbb{S}_0^M$.

Algorithm 1 The proposed set partitioning algorithm parameterized by $(M, B, J, J_{\mathrm{b}})$

1. Set M, B and J.
2. Calculate $\eta = B/J$.
3. Set J_{b} such that $J_{\mathrm{b}}\eta = \lfloor J_{\mathrm{b}}\eta \rfloor$ and $J_{\mathrm{b}} \in \{1,2,\cdots,J\}$.
4. Calculate $J_{\mathrm{it}} = \inf(\{k \mid k \in \{1,2,\cdots,J\}, k\eta = \lfloor k\eta \rfloor\})$.
5. Initialize $\mathbb{S}_J^M$ and assign $j = 0$.
6. (a) do
   (b) if $J - j \neq J_{\mathrm{b}}$
   (c) $\tilde{J} = J_{\mathrm{it}}$;
   (d) else
   (e) $\tilde{J} = J_{\mathrm{b}}$;
   (f) end
   (g) $j = j + \tilde{J}$;
   (h) $B_{\mathrm{sp}} = \tilde{J}\eta$;
   (i) $\mathbb{S}_{J-j}^{M} = \mathtt{SP}\left(\tilde{J}, B_{\mathrm{sp}}, \mathbb{S}_{J-(j-\tilde{J})}^{M}\right)$; // partition $\mathbb{S}_{J-(j-\tilde{J})}^{M}$
   (j) while $j < J$
7. Output $\mathcal{S}^{\mathrm{GTIM}} = \mathbb{S}_0^M$.

D. More Examples

1) The algorithm with $(M = 2, B = 3, J = 2, J_b = 2)$: This is the example that is previously discussed and illustrated in Fig. 7. Here, we want to connect that example with the definitions in the previous subsection. In this example, the number of loops is one as $J_{\mathrm{b}} = 2$. The algorithm 1 reduces to $\mathcal{S}^{\mathrm{GTIM}} = \mathbb{S}_0^2 = \mathtt{SP}\left(2, 3, \mathbb{S}_2^2\right)$. The steps taken in Figs. 7(a-c) are formalized as following.

The 1^{st} step (Fig. 7(a)): The first step is to partition $\mathbb{P}^{2,2}$ into $\mathbb{P}_0^{2,2}$ and $\mathbb{P}_1^{2,2}$ such that:

$$\left(\mathbb{P}_0^{2,2}, \mathbb{P}_1^{2,2}\right) = \underset{\mathbb{P}_0^{2,2}, \mathbb{P}_1^{2,2}}{\arg\max} \left\| \mathbf{d}_{\mathrm{S}}\left(\mathbb{P}_0^{2,2}\right) - \mathbf{d}_{\mathrm{S}}\left(\mathbb{P}_1^{2,2}\right) \right\| \tag{24}$$

subject to:

$$\left|\mathbb{P}_0^{2,2}\right| = \left|\mathbb{P}_1^{2,2}\right| = \lfloor (M+1)^J/2 \rfloor, \tag{25}$$

$$\mathbb{P}_0^{2,2} \neq \mathbb{P}_1^{2,2} \neq \emptyset, \mathbb{P}_0^{2,2}, \mathbb{P}_1^{2,2} \subset \mathbb{P}^{2,2} \text{ and } \mathbb{P}_0^{2,2} \cap \mathbb{P}_0^{2,2} = \emptyset. \quad (26)$$

The expression in (24) guarantees that $\mathbb{P}_0^{2,2}$ and $\mathbb{P}_1^{2,2}$ have the farthest distance with the constraints (25) and (26). The expression in (25) indicates that both set $\mathbb{P}_0^{2,2}$ and $\mathbb{P}_1^{2,2}$ must contain $\lfloor (M+1)^J/2 \rfloor$ elements. This is equivalent to:

$$\lfloor \log_2 |\mathbb{P}_0^{2,2}| \rfloor = \lfloor \log_2 |\mathbb{P}_1^{2,2}| \rfloor \geq B_{\text{sp}} - 1,$$

which means that the partitioned sets $\mathbb{P}_0^{2,2}$ and $\mathbb{P}_1^{2,2}$ can be at least represented by $B_{\text{sp}} - 1$ bits. The vectors in $\mathbb{P}_0^{2,2}$ and $\mathbb{P}_1^{2,2}$ will be assigned with the same $2^{B_{\text{sp}}-1}$ binary vectors, which will be each appended by a new binary bit as the MSB. It is intuitive that (24) can be found in the outer layer of $\mathbb{P}^{2,2}$, see Fig. 8 for more examples and observe the positions of a collection of binary vectors that differs only at the MSB. This can be seen in the red and blue markers.

The 2nd step (Fig. 7(b)): At the 2$^{\text{nd}}$ step, the sets $\mathbb{P}_0^{2,2}$ and $\mathbb{P}_1^{2,2}$ can be further partitioned into $\mathbb{P}_{0,0}^{2,2}$, $\mathbb{P}_{0,1}^{2,2}$, $\mathbb{P}_{1,0}^{2,2}$ and $\mathbb{P}_{1,1}^{2,2}$. The arrangement of all the sets is done such that $\mathbb{P}_{0,1}^{2,2}$ is the neighbor of $\mathbb{P}_{1,1}^{2,2}$ as the Hamming distance of the bits associated with both sets is 1. Doing this ensures that the MSB and the next bit position of binary vectors of $\mathbf{s}_l \in \mathbb{P}_{0,1}^{2,2}$ and $\mathbf{s}_l \in \mathbb{P}_{1,1}^{2,2}$ have the Hamming distance of 1.

The 3rd step (Fig. 7(c)): The same procedures in the 2$^{\text{nd}}$ step can be repeated in the 3$^{\text{rd}}$ step. Alternatively, we can assign the LSB of the elements of $\mathcal{S}^{\text{s}}$ and arrange it such that it differs only at 1-bit position with their neighbors. The output of the third step is the ordered set $\tilde{\mathbb{P}}^{2,2}$ as shown in Fig. 7(c). Notice that the Hamming distance between two neighboring binary vectors is 1; moreover, the Hamming distance with the next neighbors is 2 and so on. Translating these processes with respect to (19), the function SP ensures that the farther constellation point has a larger Hamming distance. Other examples with $J = 2$ and different values of M and B can be found in Fig. 8.

2) The algorithm with ($M = 2, B = 6, J = 4, J_b = 2$): Instead of $J = 2$, now we extend the previous example to $J = 4$. In this example, it can be shown that the already-defined codebook can be used to design another codebook with higher dimensions. Furthermore, the number of iterations is 2, and at each iteration $\texttt{SP}\left(2, 3, \mathbb{S}_{J-(j-2)}^{M}\right)$ is performed, which is already illustrated in Fig. 7. The output of the first iteration, i.e., $\mathbb{S}_{4-2}^{M} = \texttt{SP}\left(2, 3, \mathbb{S}_{4-0}^{M}\right)$, is given as:

$$\mathbb{S}_{4-2}^{2} = \left(\underset{000XXX}{\begin{bmatrix} \mathbf{x} \\ I_0 \\ I_0 \end{bmatrix}}, \underset{001XXX}{\begin{bmatrix} \mathbf{x} \\ m_0 \\ I_0 \end{bmatrix}}, \underset{010XXX}{\begin{bmatrix} \mathbf{x} \\ m_1 \\ m_0 \end{bmatrix}}, \underset{011XXX}{\begin{bmatrix} \mathbf{x} \\ m_1 \\ I_0 \end{bmatrix}}, \underset{100XXX}{\begin{bmatrix} \mathbf{x} \\ I_0 \\ m_0 \end{bmatrix}}, \underset{101XXX}{\begin{bmatrix} \mathbf{x} \\ I_0 \\ m_1 \end{bmatrix}}, \underset{110XXX}{\begin{bmatrix} \mathbf{x} \\ m_1 \\ m_1 \end{bmatrix}}, \underset{111XXX}{\begin{bmatrix} \mathbf{x} \\ m_0 \\ m_1 \end{bmatrix}} \right).$$

In this case, the length of the vector $\mathbf{x}$ is two. At the last iteration, we have $J_{\text{b}} = 2$ and the output is $\mathcal{S}^{\text{GTIM}} = \mathbb{S}_{4-4}^{M}$ as expressed as:

$$\mathbb{S}_{4-4}^{2} = \left(\underset{000000}{\begin{bmatrix} I_0 \\ I_0 \\ I_0 \\ I_0 \end{bmatrix}}, \underset{000001}{\begin{bmatrix} m_0 \\ I_0 \\ I_0 \\ I_0 \end{bmatrix}}, \underset{000010}{\begin{bmatrix} m_1 \\ m_0 \\ I_0 \\ I_0 \end{bmatrix}}, \underset{000011}{\begin{bmatrix} m_1 \\ I_0 \\ I_0 \\ I_0 \end{bmatrix}}, \underset{000100}{\begin{bmatrix} I_0 \\ m_0 \\ I_0 \\ I_0 \end{bmatrix}}, \underset{000101}{\begin{bmatrix} I_0 \\ m_1 \\ I_0 \\ I_0 \end{bmatrix}}, \underset{000110}{\begin{bmatrix} m_1 \\ m_1 \\ I_0 \\ I_0 \end{bmatrix}}, \underset{000111}{\begin{bmatrix} m_0 \\ m_1 \\ I_0 \\ I_0 \end{bmatrix}}, \right.$$
$$\left. \underset{001000}{\begin{bmatrix} I_0 \\ I_0 \\ m_0 \\ I_0 \end{bmatrix}}, \underset{001001}{\begin{bmatrix} m_0 \\ I_0 \\ m_0 \\ I_0 \end{bmatrix}}, \underset{001010}{\begin{bmatrix} m_1 \\ m_0 \\ m_0 \\ I_0 \end{bmatrix}}, \underset{001011}{\begin{bmatrix} m_1 \\ I_0 \\ m_0 \\ I_0 \end{bmatrix}}, \underset{001100}{\begin{bmatrix} I_0 \\ m_0 \\ m_0 \\ I_0 \end{bmatrix}}, \underset{001101}{\begin{bmatrix} I_0 \\ m_1 \\ m_0 \\ I_0 \end{bmatrix}}, \underset{001110}{\begin{bmatrix} m_1 \\ m_1 \\ m_0 \\ I_0 \end{bmatrix}}, \underset{001111}{\begin{bmatrix} m_0 \\ m_1 \\ m_0 \\ I_0 \end{bmatrix}}, \dots \right).$$

Notice that the vector $\mathbf{x}$ is replaced with the result as depicted in Fig. 7(c), and the binary representation is appended by replacing the LSBs with new ordered binary vectors.

3) The algorithm with ($M = 3, B = 6, J = 3, J_b = 2$): The main purpose of this example is to visualize the modularity of the algorithm. At the first iteration, the process $\mathbb{S}_{3-1}^{3} = \texttt{SP}\left(1, 2, \mathbb{S}_{3-0}^{3}\right)$ is carried out. The output can be expressed as in (23). Visually, it is equivalent to order and label the symbol s_2 in $\mathcal{S}^{\text{GTIM}}$, which can be shown in Fig. 9 along s_2-axis. Then, on each plane with respect to the s_2-axis, $\mathcal{S}^{\text{GTIM}} = \mathbb{S}_{3-3}^{3} = \texttt{SP}\left(2, 4, \mathbb{S}_{3-1}^{3}\right)$ is performed. Notice that the constellation for $\texttt{SP}\left(2, 4, \mathbb{S}_{3-1}^{3}\right)$ is shown in Fig. 8(b). Therefore, the final result can be seen in Fig. 9, which shows the arrangement of Fig. 8(b) on each plane. The location of each plane is denoted by (23), which is carried out in the first iteration, i.e., $\texttt{SP}\left(1, 2, \mathbb{S}_{3-0}^{3}\right)$.

E. Optimality Discussion

First, we will discuss the effect of J_{b}, which parameterizes algorithm 1. Recall that the arrangement in Fig. 8(c) has $J_{\text{b}} = 2$. Alternatively, we can also set $J_{\text{b}} = 1$ for the same problem. The result is shown in Fig. 10(a). It is obvious that the arrangement in Fig. 10(a) has a worse BER compared to Fig. 8(c). An easy way to see this is by looking at pairs of symbols that have the Hamming distance of 2. There are pairs with the Hamming distance of 2 in Fig. 10(a) that have a smaller Euclidean distance than that of Fig. 8(c). Furthermore, we can also find the same observation with $J_{\text{b}} = 3$ and $J_{\text{b}} = 2$. In this paper, we claim that with respect to (19) the proposed algorithm is suboptimal and a detailed optimality discussion will be left for future studies. For a certain case such as the arrangement in Fig. 8(b), which resembles that of 16-QAM, Lemma 9 in [31] can be used to prove the optimality. However, for a general $J > 2$ Lemma 9 in [31] cannot be directly applied. Following [31], some definitions and trivial operations such as the average distance spectrum, binary and codeword permutation needs to be defined first. The proposed algorithm gives a trade-off between the exhaustive search with the search size as defined in (18) and a good set of $\mathcal{S}^{\text{GTIM}}$ in terms of the Euclidean and Hamming distances.

It is also worth discussing here that if $|m_0 - I_0| < |m_i - m_j|, \forall i \neq j \in \{0, 1, \cdots, M-1\}$ then the BER is limited by $|m_0 - I_0|$. Therefore, in order to maintain the BER gain of SC-GTIM, a minor modification for the function SP is required.

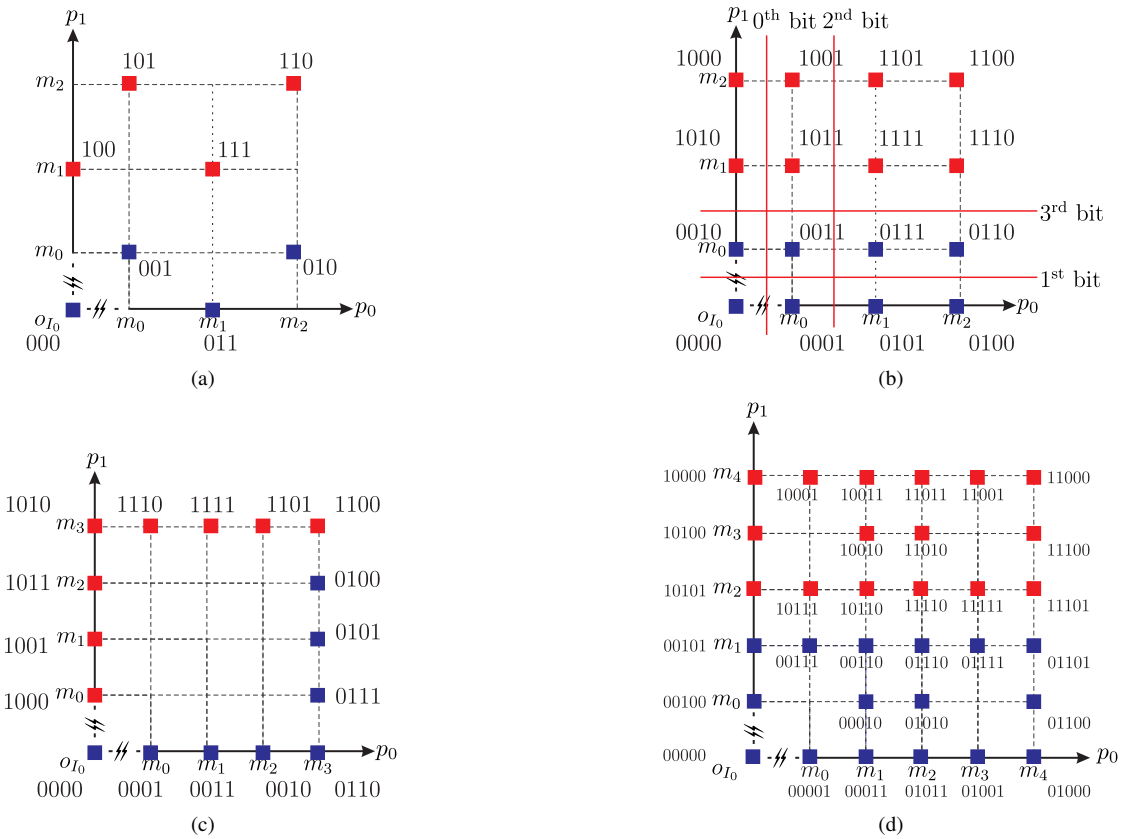

Fig. 8. $\mathtt{SP}(\cdot)$ with: (a) $M = 3$, $B = 3$ and $\eta = 1.5$; (b) $M = 3$, $B = 4$ and $\eta = 2$; (c) $M = 4$, $B = 4$ and $\eta = 2$; (d) $M = 5$, $B = 5$ and $\eta = 2.5$.

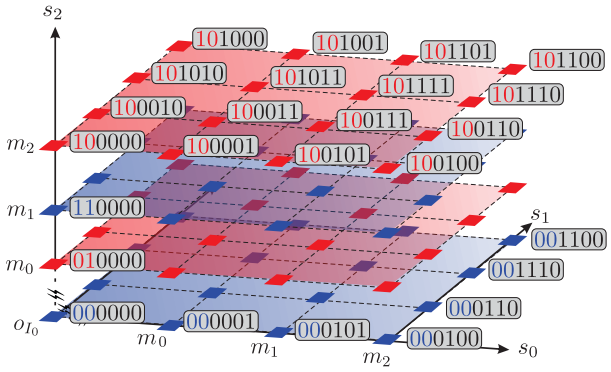

Fig. 9. An illustration for the proposed algorithm with $(3, 6, 3, 2)$.

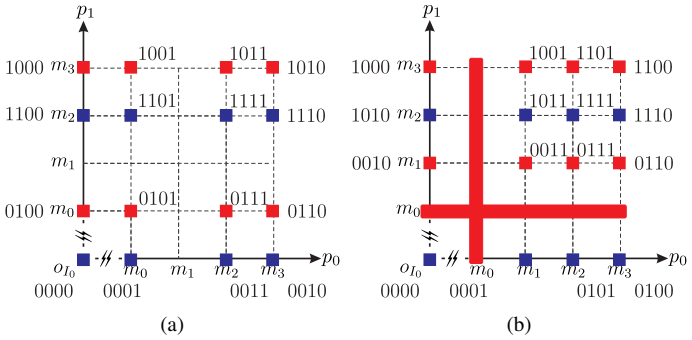

Fig. 10. (a) An output of algorithm 1 with (4,4,2,1) and (b) a modified construction of Fig. 8(c) if $|m_0 - I_0| < |m_i - m_j|, \forall i \neq j \in \{0, 1, \cdots, M-1\}$.

The modification is carried out such that the set $\mathbb{P}_{\mathrm{dc}}^{M,\tilde{J}}$ is predefined to include the vectors $\mathbf{p} \in \mathbb{P}^{M,\tilde{J}}$ that contain the value m_0. It means that the vectors containing the value m_0 are not used. Fig. 10(b) illustrates the aforementioned modification with the red cross, which denotes the unused vectors.

V. Results and Discussion

A. Simulation Setup

In order to compare different results with different I_0, a ratio υ is defined as follows:

$$\upsilon = \frac{I_{\mathrm{a}} - I_0}{d_{\min,M}}, \tag{27}$$

where $d_{\min,\mathrm{M}}$ denotes the minimum distance of the conventional M-PAM and defined as $d_{\min,\mathrm{M}} = (I_{\mathrm{b}} - I_{\mathrm{a}})/(M-1)$. The case where $\upsilon > 1$ shows that the $|I_{\mathrm{a}} - I_0|$ is greater than the minimum distance of the conventional M-PAM. As the performance gains of SC-TIM and SC-GTIM compared to the SC-PAM depend on υ, we are interested in two different cases, which are $\upsilon < 1$ (namely $C_{\upsilon<1}$) and $\upsilon > 1$ (namely $C_{\upsilon>1}$). The case $C_{\upsilon>1}$ is the case where the LED is allowed

Table I. Simulation Parameters

Parameters	Notation	Values	Unit
3-dB LED bandwidth	f_{led}	35	MHz
LED Lambertian order	m	1	-
PD's responsivity	R	0.7	A/W
PD's gain	M	50	-
PD's FoV	FoV	90°	-
PD's effective detection area	A_{AP}	1	cm^2
Symbol rate	R_{s}	50	MSymb/s
FFT size	N	32	-
FEC threshold	$P_{\text{b,target}}$	3.8×10^{-3}	-

to be completely off during the transmission, i.e., $I_0 = 0$. On the other hand, the case $C_{\upsilon<1}$ is the case where $I_0 \neq 0$ and the distance between I_{a} and I_0 is smaller than the minimum distance of SC-PAM. This is when the SC-TIM can be worse than SC-PAM. In general, the cases $C_{\upsilon>1}$ and $C_{\upsilon<1}$ are defined to show extreme performance gains of SC-TIM and SC-GTIM, i.e., significant BER gains are achieved in $C_{\upsilon>1}$ and slight BER gains are achieved in the other case.

For our simulation setup, the characteristic of a high-speed IR LED VSMY3940X01 [40] is used to have a practical linear dynamic range value. Fitting the $P-I$ curve with the 5^{th}-order polynomial function, we observe that $I_{\text{a}} = 600$ mA and $I_{\text{b}} = 800$ mA. As for the I_0, we pick $I_0 = 0$ for $C_{\upsilon>1}$ and $I_0 = 550$ mA for $C_{\upsilon<1}$ with $M \in \{2,4\}$. The reason for this is to show the dependency of I_0 and the performance gains of SC-TIM and SC-GTIM.

Other parameter values are shown in Table. I. The LED is modeled as a first order Butterworth filter with the 3-dB bandwidth $f_{\text{led}} = 35$ MHz. The LED Lambertian order for the optical channel calculation in (5) as $m = 1$. The ADC is modeled as a zero-order hold with a fifth order Bessel lowpass filter (LPF) whose 3-dB bandwidth is $R_{\text{s}}(L_{\text{cp}}+N)/(2N)$. The PD's responsivity is chosen to be $R = 0.7$ A/W based on, for example, [41]. Lastly, the FFT size is chosen to be $N = 32$ [36] and the BER target used in this paper is 3.8×10^{-3} [42].

For the optical channel setup, the vertical and horizontal distances between the UE and the AP are set to be $d_{\text{v}} = 1.6$ m and $d_{\text{h}} = 1.55$ m, respectively. For the orientation of the UE, we set θ to be 27.75, see the configuration C_1 in [34, Fig. 7].

The room dimensions are assumed to be $5\times3.5\times3$ m^3. The reflectivities of the walls are assumed to be 0.3, the reflectivity of the ceiling is 0.69, and the reflectivity of the floor is 0.09. The reflectivities of the surfaces of the rectangular prism modeling the human body are assumed to be 0.6 with the exception of the upper surface, which is 0.9. In addition, the resolution of the partition is 10 to generate the optical CIR [33]. A more detailed discussion and explanation as to where these values are taken from can be found in [32], [34].

B. Error Performance

The BER comparisons are shown in Fig. 11. All APEPs are shown by solid lines to avoid confusion. The reason for using the solid lines for all APEPs is that the upper bounds are sufficiently tight, but not exactly equal, with each corresponding simulation result. The simulation results are shown with different markers. Note that for fair comparisons, the set $\mathcal{S}^{\text{TIM}}$ is also constructed based on a Gray code and exhaustive search. Fig. 11(a) shows the advantages of SC-GTIM over both SC-PAM and SC-TIM. Approximately 2 dB gain can be achieved by SC-TIM with $J = 2$ compared to SC-PAM. To show the performance of SC-TIM with $J = 4$, the constellation size needs to be increased due to the limitation of vectors in $\mathcal{S}^{\text{s}}$ that can be chosen by SC-TIM. In order to obtain $\eta = 1$ with $J = 4$, the parameters M and K of the SC-TIM should be set as $M = 4$ and $K = 1$. As the minimum distance in the interval $[I_{\text{a}}, I_{\text{b}}]$ narrows, the BER performance of SC-TIM is worse than that of SC-PAM. On the other hand, as SC-GTIM can chose arbitrary vectors in $\mathcal{S}^{\text{s}}$, approximately 10 dB gain can be obtained. It is also shown that even by increasing η to be $\eta = 1.5$, the BER of SC-GTIM is still better than SC-PAM and SC-TIM.

In Fig. 11(a)-(d), we also show the results of the case when increasing J for SC-GTIM does not change the BER performance. This means that by using the proposed set partitioning algorithm, the average minimum distance does not change significantly. This also means that the design problem for higher dimension J can be reduced to design a good set $\mathcal{S}^{\text{GTIM}}$ for $J = 2$ which will reduce the memory complexity. This issue will be discussed in the next subsection.

In Fig. 11(b), it can be seen that the performance of SC-TIM with $\eta = 2$ is better with respect to SC-PAM compared to those with $\eta = 1$. For SC-GTIM, the BER gain decreases, but it is still significantly better than the others, i.e., approximately 5 dB better. In Fig. 8(b) and (c), it is shown that for $J = 2$, $\eta = 2$ can be achieved by either $M = 3$ and $M = 4$. The results in Fig. 11(b) show that we can take advantage of the fact that $|I_0 - I_{\text{a}}| > d_{\min,M}$. That is, as the same η can be achieved by a lower constellation size, the lower constellation size should be chosen for designing the set $\mathcal{S}^{\text{GTIM}}$. The reason for this is simply because of $d_{\min,4} < d_{\min,3}$. In addition, we also observe that about 2 dB gain with respect to SC-PAM can still be achieved for SC-GTIM with $\eta = 3$.

The results for the case $C_{\upsilon<1}$ are shown in Fig. 11(c) and (d). At $\eta = 1$, Fig. 11(c) shows the limitation of SC-TIM. As shown in Fig. 5(c), the BER is limited by two constellation points near o_{I_o}. This problem can be averaged out by increasing J, see (12). However, for SC-TIM with $J = 4$, the problem with $d_{\min,4} < d_{\min,2}$ also appears in Fig. 11(a); hence, the BER is still worse compared to that of SC-PAM. On the contrary, the advantage of SC-GTIM over the others is still maintained.

The limitation of SC-GTIM is shown in Fig. 11(d). To maintain the BER gain, it is clear that SC-GTIM cannot use the constellation diagram in Fig. 8(b) as the minimum distance is limited by all constellation points near I_0, which will result in a worse BER performance compared to SC-PAM and SC-TIM. However, due to the flexibility of SC-GTIM, the constellation diagram in Fig. 8(c) can be modified to be that as shown in Fig. 10(b). As the constellation points near I_0 acts as the limitation, the vectors $\mathbf{s}_l$ that contains the symbol I_{a} will not be picked. Therefore, the same structure in Fig. 8(b) can be used in Fig. 8(c) by not picking $s_j = I_{\text{a}}, \forall j$. The result is that the BER gain can still be achieved even though it is small.

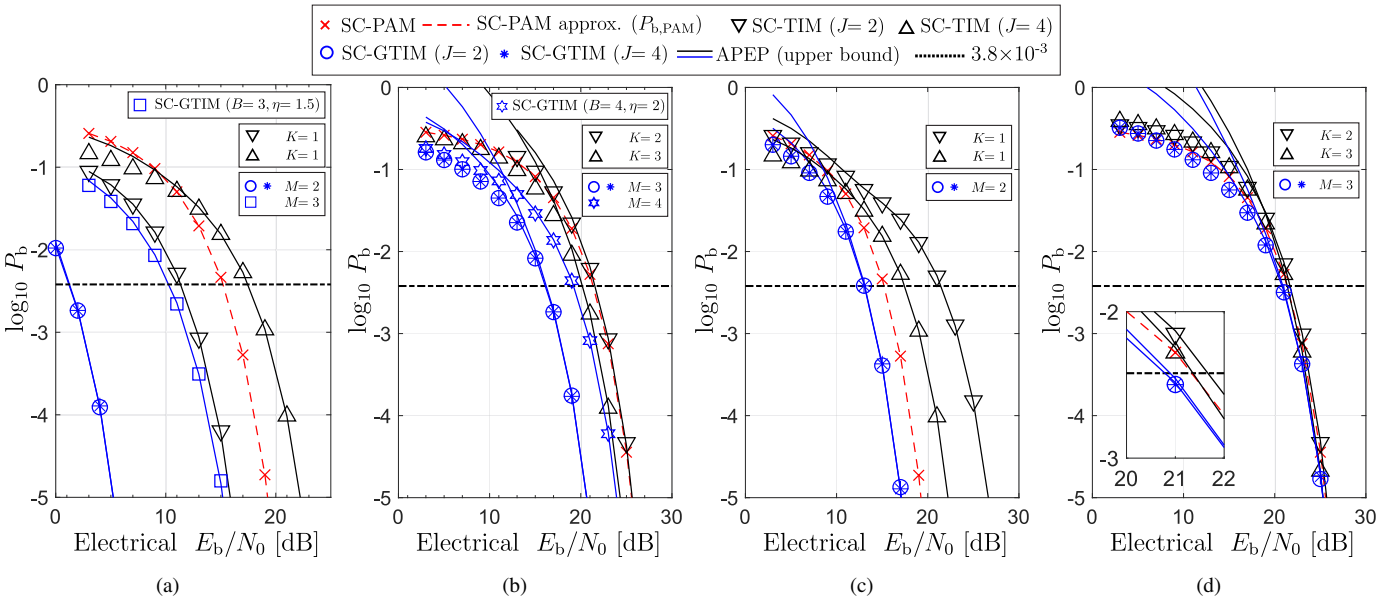

Fig. 11. BER comparisons for: (a) $C_{\upsilon>1}$ and $\eta = 1$; (b) $C_{\upsilon>1}$ and $\eta = 2$; (c) $C_{\upsilon<1}$ and $\eta = 1$; and (d) $C_{\upsilon<1}$ and $\eta = 2$.

C. Complexity and PAPR Penalties

At first, one might think that the brute-force search is the main reason for the additional complexity. In fact, the computational complexities of SC-TIM and SC-GTIM are the same as the conventional one if the Voronoi region is used provided that the total transmitted bits B_t is the same. Fig. 8(b) is used as an example. The goal is to decode the binary vector $[0011]^{\mathrm{T}}$. Using the Voronoi region shown by red solid lines (only regions of interest are shown), the MSB (the 3$^{\mathrm{rd}}$ bit) can be decoded first. This can easily be done based on the location of the estimated s_1, namely $\hat{s}_1$, and the boundary $(m_0 + m_1)/2$. In addition, the operation is done over a single real value to allow a fair comparison with the SC-PAM. The rest of the bits, i.e., the 2$^{\mathrm{nd}}$ to the 0$^{\mathrm{th}}$ bits, can be estimated in the same way. Hence, the computational complexity is $O(B)$ and the same as the SC-PAM.

As previously discussed after (7) and (11), it cannot be guaranteed that the single-tap FDE can be applied to SC-TIM and SC-GTIM systems. We observe that this is true for SC-TIM with $J > 1$ since the matrix $\mathbf{R_s}$ is not circulant. On the contrary, there are certain $\mathcal{S}^{\mathrm{GTIM}}$ such that $\mathbf{R_s}$ is circulant. For example, $\mathbf{R_s}$ with the arrangements shown in Fig. 8(b) and Fig. 9 have a circulant $\mathbf{R_s}$. Generally, if:

$$\eta \in \mathbb{Z}^+ \text{ and } M = 2^{\eta} - 1, \tag{28}$$

then $\mathbf{R_s}$ will be circulant. A simple explanation for this is that for an equally-likely binary digit $\{0, 1\}$, then all symbols will be equally-likely selected if (28) is satisfied. Hence, in terms of relative distances between constellation symbols, the constellation resembles that of SC-PAM whose $\mathbf{R_s}$ is circulant. If the single-tap FDE can be applied, the computational complexity is $O\left(2N \log_2 N\right)$. Otherwise, it is $O\left(2N^2\right)$.

The complexity penalties come from the mapping of bits to the symbol, which is the size of the lookup tables (LUTs) used to store the sets $\mathcal{S}^{\mathrm{TIM}}$ and $\mathcal{S}^{\mathrm{GTIM}}$. The case when $J = 1$ is used in order for SC-PAM to have a fair comparison. For SC-PAM, the memory complexity is $O\left(2^B\right)$. For SC-TIM and SC-GTIM, the complexity is $O\left(J2^B\right)$ as the LUT is now a matrix. As previously mentioned, the BER performance of SC-GTIM can be invariant with respect to J due to the fact that the minimum distance is the same. In this case, the memory complexity of SC-GTIM can be limited to $O(2^{B+1})$.

Table II. PAPR Comparisons

	SC-PAM	SC-TIM	SC-GTIM
$\eta = 1$	0.57 dB	2.59 dB	2.02 dB
$\eta = 2$	0.58 dB	1.83 dB	1.8 dB

For PAPR comparisons, given the linear dynamic range $[I_a, I_b]$ and the new degree of freedom $I_0 < I_a$, it is obvious that the average energy per symbols of both SC-TIM and SC-GTIM are lower; consequently, the PAPR increases as the peak value remains the same. However, I_0 can also be set such that $I_b < I_0$. In this case, the PAPR does not always increase depending on $|I_0 - I_b|$.

For PAPR comparisons, we only present the configurations which give the best BER performances in Fig. 11. In addition, only the case $C_{\upsilon>1}$ is of interest as it gives a higher PAPR compared to that of the other case. Table. II summarized the PAPR comparisons. As previously mentioned before, the PAPRs of either SC-TIM and SC-GTIM are higher due to the fact that the average energy per symbol decreases. For a certain configuration of SC-TIM, when the symbol I_0 is picked more frequently than in SC-GTIM, SC-GTIM has a lower PAPR compared to SC-TIM; hence, the average energy per symbol of SC-TIM is lower than that of SC-GTIM.

VI. Conclusions

This paper investigated the implementation of IM in single-carrier PAM with block transmission for OWC. Specifically, we compared PAM (SC-PAM) and SC-TIM with the proposed SC-GTIM. The main difference between SC-TIM and SC-GTIM was the flexibility in choosing an arbitrary number of

active time slots. Specifically, only predefined K time slots were active for SC-TIM, while there was no fixed K for SC-GTIM. We showed that this flexibility in choosing the number of active time slots was used to mitigate the performance limitations of SC-TIM due to the linear dynamic range of LEDs. A set partitioning algorithm was also proposed to construct a codebook for SC-GTIM. In terms of BER, it was shown that more than a 3 dB gain could be achieved by SC-GTIM. In terms of maximum achievable spectral efficiency for a given constellation size M, it was also shown that SC-GTIM achieved better performance than the others. This was especially true in low-to-moderate spectral efficiency scenarios, where a 50% improvement could be achieved compared to SC-PAM. In terms of computational complexity penalties, we showed that there was a memory complexity penalty for both SC-TIM and SC-GTIM compared to that of SC-PAM due to the fact that the size of the codebook for mapping from bits to symbols was larger. In addition, there was also a PAPR penalty as the average energy per symbols for SC-TIM and SC-GTIM were lower than that of SC-PAM, while the maximum of the average transmitted energy was the same.

REFERENCES

[1] A. A. Purwita, A. Yesilkaya, T. Cogalan, M. Safari, and H. Haas, "Generalized time slot index modulation for LiFi," in *2019 IEEE 30th Annual International Symposium on Personal, Indoor and Mobile Radio Communications (PIMRC)*, Istanbul, Turkey, Sep. 2019, pp. 1–7.

[2] "Cisco visual networking index: Global mobile data traffic forecast update, 2016-2021 white paper," White Paper, Cisco, March 2017.

[3] M. K. Samimi and T. S. Rappaport, "3-D millimeter-wave statistical channel model for 5G wireless system design," *IEEE Transactions on Microwave Theory and Techniques*, vol. 64, no. 7, pp. 2207–2225, July 2016.

[4] S. Priebe and T. Kürner, "Stochastic modeling of THz indoor radio channels," *IEEE Transactions on Wireless Communications*, vol. 12, no. 9, pp. 4445–4455, September 2013.

[5] T. Koonen, "Indoor optical wireless systems: Technology, trends, and applications," *Journal of Lightwave Technology*, vol. 36, no. 8, pp. 1459–1467, April 2018.

[6] I. Stefan, H. Burchardt, and H. Haas, "Area spectral efficiency performance comparison between VLC and RF femtocell networks," in *2013 IEEE International Conference on Communications (ICC)*, Budapest, Hungary, June 2013, pp. 3825–3829.

[7] H. Haas, L. Yin, Y. Wang, and C. Chen, "What is LiFi?" *Journal of Lightwave Technology*, vol. 34, no. 6, pp. 1533–1544, March 2016.

[8] R. Mesleh, H. Haas, C. W. Ahn, and S. Yun, "Spatial modulation - a new low complexity spectral efficiency enhancing technique," in *2006 First International Conference on Communications and Networking in China*, Beijing, China, Oct 2006, pp. 1–5.

[9] R. Y. Mesleh, H. Haas, S. Sinanovic, C. W. Ahn, and S. Yun, "Spatial modulation," *IEEE Transactions on Vehicular Technology*, vol. 57, no. 4, pp. 2228–2241, July 2008.

[10] R. Abu-alhiga and H. Haas, "Subcarrier-index modulation OFDM," in *2009 IEEE 20th International Symposium on Personal, Indoor and Mobile Radio Communications*, Tokyo, Japan, Sept 2009, pp. 177–181.

[11] M. Nakao, T. Ishihara, and S. Sugiura, "Single-carrier frequency-domain equalization with index modulation," *IEEE Communications Letters*, vol. 21, no. 2, pp. 298–301, Feb 2017.

[12] J. Choi, "Single-carrier index modulation and CS detection," in *2017 IEEE International Conference on Communications (ICC)*, Paris, France, May 2017, pp. 1–6.

[13] W. O. Popoola, E. Poves, and H. Haas, "Error performance of generalised space shift keying for indoor visible light communications," *IEEE Transactions on Communications*, vol. 61, no. 5, pp. 1968–1976, May 2013.

[14] H. Haas and R. I. T. Abu-Alhiga, "Encoding method by conveying coded bit information on patterns of different modulation schemes on orthogonal resource units," European Patent EP2 476 210B1, Jan. 27, 2016.

[15] E. Basar, "Orbital angular momentum with index modulation," *IEEE Transactions on Wireless Communications*, vol. 17, no. 3, pp. 2029–2037, March 2018.

[16] E. Basar, M. Wen, R. Mesleh, M. D. Renzo, Y. Xiao, and H. Haas, "Index modulation techniques for next-generation wireless networks," *IEEE Access*, vol. 5, pp. 16 693–16 746, 2017.

[17] S. Sugiura, T. Ishihara, and M. Nakao, "State-of-the-art design of index modulation in the space, time, and frequency domains: Benefits and fundamental limitations," *IEEE Access*, vol. 5, pp. 21 774–21 790, 2017.

[18] N. Ishikawa, S. Sugiura, and L. Hanzo, "50 years of permutation, spatial and index modulation: From classic RF to visible light communications and data storage," *IEEE Communications Surveys Tutorials*, vol. 20, no. 3, pp. 1905–1938, thirdquarter 2018.

[19] A. Nuwanpriya, S. W. Ho, J. A. Zhang, A. J. Grant, and L. Luo, "PAM-SCFDE for optical wireless communications," *Journal of Lightwave Technology*, vol. 33, no. 14, pp. 2938–2949, July 2015.

[20] M. Khalighi, S. Long, S. Bourennane, and Z. Ghassemlooy, "PAM- and CAP-based transmission schemes for visible-light communications," *IEEE Access*, vol. 5, pp. 27 002–27 013, 2017.

[21] L. Bosotti and G. Pirani, "A PAM-PPM signalling format in optical fibre digital communications," *Optical and Quantum Electronics*, vol. 11, no. 1, pp. 71–86, Jan 1979.

[22] M. A. Herro and L. Hu, "A new look at coding for APD-based direct-detection optical channels," *IEEE Transactions on Information Theory*, vol. 34, no. 4, pp. 858–866, July 1988.

[23] H. Sugiyama and K. Nosu, "MPPM: a method for improving the band-utilization efficiency in optical PPM," *Journal of Lightwave Technology*, vol. 7, no. 3, pp. 465–472, March 1989.

[24] H. Zhang and T. A. Gulliver, "Pulse position amplitude modulation for time-hopping multiple access UWB communications," in *2004 IEEE Wireless Communications and Networking Conference (IEEE Cat. No.04TH8733)*, vol. 2, Atlanta, GA, USA, USA, March 2004, pp. 895–900 Vol.2.

[25] W. Huang, C. Tsai, and P. Ting, "Optimal amplitude design for MN-ary pulse position amplitude modulation," in *2012 IEEE Vehicular Technology Conference (VTC Fall)*, Quebec City, QC, Canada, Sept 2012, pp. 1–5.

[26] A. Tyagi and R. Bose, "A new distance notion for PPAM space–time trellis codes for UWB MIMO communications," *IEEE Transactions on Communications*, vol. 55, no. 7, pp. 1279–1282, July 2007.

[27] G. Ungerboeck, "Channel coding with multilevel/phase signals," *IEEE Transactions on Information Theory*, vol. 28, no. 1, pp. 55–67, Jan 1982.

[28] Y. Zeng, R. Green, and M. Leeson, "Multiple pulse amplitude and position modulation for the optical wireless channel," in *2008 10th Anniversary International Conference on Transparent Optical Networks*, vol. 4, Athens, Greece, June 2008, pp. 193–196.

[29] S. Jacob, T. L. Narasimhan, and A. Chockalingam, "Space-time index modulation," in *2017 IEEE Wireless Communications and Networking Conference (WCNC)*, San Francisco, CA, USA, March 2017, pp. 1–6.

[30] Proakis, *Digital Communications 5th Edition*. McGraw Hill, 2007.

[31] E. Agrell, J. Lassing, E. G. Strom, and T. Ottosson, "On the optimality of the binary reflected Gray code," *IEEE Transactions on Information Theory*, vol. 50, no. 12, pp. 3170–3182, Dec 2004.

[32] J. M. Kahn and J. R. Barry, "Wireless infrared communications," *Proceedings of the IEEE*, vol. 85, no. 2, pp. 265–298, Feb 1997.

[33] H. Schulze, "Frequency-domain simulation of the indoor wireless optical communication channel," *IEEE Transaction on Communications*, vol. 64, no. 6, pp. 2551–2562, June 2016.

[34] A. A. Purwita, M. D. Soltani, M. Safari, and H. Haas, "Terminal orientation in OFDM-based LiFi systems," *IEEE Transactions on Wireless Communications*, vol. 18, no. 8, pp. 4003–4016, Aug 2019.

[35] M. D. Soltani, A. A. Purwita, Z. Zeng, H. Haas, and M. Safari, "Modeling the random orientation of mobile devices: Measurement, analysis and LiFi use case," *IEEE Transactions on Communications*, vol. 67, no. 3, pp. 2157–2172, March 2019.

[36] A. A. Purwita, C. Chen, M. Safari, and H. Haas, "Cyclic-prefixed system with PAM using DFE and THP for uplink transmission in LiFi," in *2019 IEEE International Conference on Communications (ICC)*, Shanghai, China, 2019.

[37] T. Fath and H. Haas, "Performance comparison of MIMO techniques for optical wireless communications in indoor environments," *IEEE Transactions on Communications*, vol. 61, no. 2, pp. 733–742, February 2013.

[38] H. V. Poor and S. Verdu, "Probability of error in MMSE multiuser detection," *IEEE Transactions on Information Theory*, vol. 43, no. 3, pp. 858–871, May 1997.

[39] S. Verdu, "Spectral efficiency in the wideband regime," *IEEE Transactions on Information Theory*, vol. 48, no. 6, pp. 1319–1343, June 2002.
[40] Vishay®. (2014, June) High speed infrared emitting diode, 940 nm, surface emitter technology. [Online]. Available: https://www.vishay.com/docs/84220/vsmy3940x01.pdf
[41] Hamamatsu Photonics K.K. (2017, September) Si APD (avalanche photodiode). [Online]. Available: https://www.hamamatsu.com/resources/pdf/ssd/si_apd_kapd0001e.pdf
[42] ITU, "Forward error correction for high bit-rate DWDM submarine systems," *ITU G.975.1*, 2004.

Ardimas Andi Purwita (S'15) received the B.S. and M.Sc. degrees in electrical engineering from the Institut Teknologi Bandung, Bandung, Indonesia, in 2011 and 2014, respectively. He is currently pursuing the Ph.D. degree with The University of Edinburgh, Edinburgh, U.K. He was with the School of Information Science, Japan Advanced Institute of Science and Technology, in 2015, as a Researcher. His current research interests include channel coding, optical wireless communication, hybrid WiFi-LiFi, and LiFi standard (IEEE 802.11bb).

Anil Yesilkaya (S'11) received the B.Sc. (Hons.) and M.Sc. degrees in electronics engineering from Kadir Has University, Istanbul, Turkey, in 2014 and 2016, respectively. He is currently pursuing the Ph.D. degree in digital communications with The University of Edinburgh. His research interests include multiple-input multiple-output optical wireless communications (MIMO-OWC) and LiFi-based in-flight connectivity. He was a recipient of the Best Paper Award at the IEEE International Conference on Communications (ICC) in 2018.

Majid Safari (S'08–M'11) Majid Safari (S'08-M'11) received his Ph.D. degree in Electrical and Computer Engineering from the University of Waterloo, Canada in 2011. He also received his B.Sc. degree in Electrical and Computer Engineering from the University of Tehran, Iran, in 2003, M.Sc. degree in Electrical Engineering from Sharif University of Technology, Iran, in 2005.

He is currently a senior lecturer (Associate Professor) in the Institute for Digital Communications at the University of Edinburgh. Before joining Edinburgh in 2013, He held postdoctoral fellowship at McMaster University, Canada. Dr. Safari is currently an associate editor of IEEE Transactions on Communications and was the TPC co-chair of the 4th International Workshop on Optical Wireless Communication in 2015. His main research interest is the application of information theory and signal processing in optical communications including fiber-optic communication, free-space optical communication, visible light communication, and quantum communication.

Harald Haas (S'98–AM'00–M'03–SM'16–F'17) received the Ph.D. degree from The University of Edinburgh in 2001. He is currently the Chair of Mobile Communications at The University of Edinburgh, and he is the Initiator, Co-Founder, and Chief Scientific Officer of pureLiFi Ltd., and the Director of the LiFi Research and Development Centre, The University of Edinburgh. He has authored 500 conference and journal papers. His main research interests are in optical wireless communications, hybrid optical wireless and RF communications, spatial modulation, and interference coordination in wireless networks.

He is an Associate Editor of the IEEE Journal of Lightwave Technologies. He gave two TED Global talks "Wireless Data From Every light Bulb" and "Forget Wi-Fi: Meet the New Li-Fi Internet" which together have been downloaded more than 5.5 million times. In 2012 and 2017, he was a recipient of the prestigious Established Career Fellowship from the Engineering and Physical Sciences Research Council (EPSRC) in the U.K. In 2014, he was selected by EPSRC as one of ten Recognizing Inspirational Scientists and Engineers Leaders in the U.K. He was a co-recipient of the EURASIP Best Paper Award for the Journal on Wireless Communications and Networking in 2015 and the Jack Neubauer Memorial Award of the IEEE Vehicular Technology Society. In 2016, he received the Outstanding Achievement Award from the International Solid State Lighting Alliance. He was a co-recipient of recent best paper awards at VTC-Fall, 2013, VTC-Spring 2015, ICC 2016, ICC 2017 and ICC 2018. In 2019 he received the James Evans Avant Garde Award of the IEEE Vehicular Technology Society. Haas is a Fellow of the Royal Academy of Engineering.